ABSTRACT

Title of Document: NONINVASIVE NEURAL DECODING OF OVERT AND COVERT HAND MOVEMENT

Trent J. Bradberry, Doctor of Philosophy, 2010

Directed By: Associate Professor José L. Contreras-Vidal, Department of Kinesiology, Graduate Program in Neuroscience and Cognitive Science, Fischell Department of Bioengineering

It is generally assumed that the signal-to-noise ratio and information content of neural data acquired noninvasively via magnetoencephalography (MEG) or scalp electroencephalography (EEG) are insufficient to extract detailed information about natural, multi-joint movements of the upper limb. If valid, this assumption could severely limit the practical usage of noninvasive signals in brain-computer interface (BCI) systems aimed at continuous complex control of arm-like prostheses for movement impaired persons. Fortunately this dissertation research casts doubt on the veracity of this assumption by extracting continuous hand kinematics from MEG signals collected during a 2D center-out drawing task (Bradberry et al. 2009, *NeuroImage*, 47:1691-700) and from EEG signals collected during a 3D center-out reaching task (Bradberry et al. 2010, *Journal of Neuroscience*, 30:3432-7). In both studies, multiple regression was performed to find a matrix that mapped past and current neural data from multiple sensors to current hand kinematic data (velocity). A novel method was subsequently devised that incorporated the weights of the mapping matrix and the standardized low resolution electromagnetic tomography (sLORETA) software to reveal that the brain sources that encoded hand kinematics in the MEG and EEG studies were corroborated by more traditional studies that required averaging across trials and/or subjects. Encouraged by the

favorable results of these off-line decoding studies, a BCI system was developed for on-line decoding of covert movement intentions that provided users with real-time visual feedback of the decoder output. Users were asked to use only their thoughts to move a cursor to acquire one of four targets on a computer screen. With only one training session, subjects were able to accomplish this task. The promising results of this dissertation research significantly advance the state-of-the-art in noninvasive BCI systems.

NONINVASIVE NEURAL DECODING OF OVERT AND COVERT HAND MOVEMENT

By

Trent J. Bradberry

Dissertation submitted to the Faculty of the Graduate School of the
University of Maryland, College Park in partial fulfillment
of the requirements for the degree of
Doctor of Philosophy
2010

Advisory Committee:

Associate Professor José L. Contreras-Vidal, Chair
Professor Bradley D. Hatfield
Professor Emeritus Arthur T. Johnson
Assistant Professor Sameer B. Shah
Assistant Professor Jae Kun Shim
Professor Yang Tao

Dedication

This dissertation is dedicated to my wife Marietta.

Acknowledgements

I would like to thank my dissertation advisor José (Pepe) Contreras-Vidal for his most valuable guidance, support, and mentorship during the entire process of conducting this dissertation research, Rodolphe Gentili and Feng Rong for their major contributions to this research and coauthorship on the journal publications that constitute the majority of this dissertation, Bruce Swett and Allen Braun for their advice, and the participants of the studies.

Table of Contents

List of Tables

List of Figures

Chapter 1: Decoding center-out hand velocity from MEG signals during visuomotor adaptation

Chapter 2: Reconstructing three-dimensional hand movements from noninvasive electroencephalographic signals

Chapter 3: A noninvasive brain-computer interface system with efficient decoder calibration based on observation of cursor movement

Chapter 1: Decoding center-out hand velocity from MEG signals during visuomotor adaptation

The material contained in this chapter is published as Bradberry TJ, Rong F, Contreras-Vidal JL (2009) Decoding center-out hand velocity from MEG signals during visuomotor adaptation. NeuroImage 47:1691–1700. Supplemental material in the journal publication has been incorporated into the main text of this dissertation chapter.

Abstract

During reaching or drawing, the primate cortex carries information about the current and upcoming position of the hand. Researchers have decoded hand position, velocity, and acceleration during center-out reaching or drawing tasks from neural recordings acquired invasively at the microscale and mesoscale levels. Here we report that we can continuously decode information about hand velocity at the macroscale level from magnetoencephalography (MEG) data acquired from the scalp during a center-out drawing task with an imposed hand-cursor rotation. The grand mean (n = 5) correlation coefficients (CCs) between measured and decoded velocity profiles were 0.48, 0.40, 0.38, and 0.28 for the horizontal dimension of movement and 0.32, 0.49, 0.56, and 0.23 for the vertical dimension of movement where the order of the CCs indicates pre-exposure, early-exposure, late-exposure, and post-exposure to the hand-cursor rotation. By projecting the sensor contributions to decoding onto whole-head scalp maps, we found

that a macroscale sensorimotor network carries information about detailed hand velocity and that contributions from sensors over central and parietal scalp areas change due to adaptation to the rotated environment. Moreover, a 3-D linear estimation of distributed current sources using standardized low-resolution brain electromagnetic tomography (sLORETA) permitted a more detailed investigation into the cortical network that encodes for hand velocity in each of the adaptation phases. Beneficial implications of these findings include a noninvasive methodology to examine the neural correlates of behavior on a macroscale with high temporal resolution and the potential to provide continuous, complex control of a noninvasive neuromotor prosthesis for movement-impaired individuals.

Introduction

In the last several decades, great strides have been made in revealing how the primate cortex may encode the current and upcoming position of the hand in space during reaching or drawing (Scott 2008). In addition to contributing to the body of neuroscientific knowledge, these discoveries have begun to beneficially impact society. Greater elucidation of the neural code for hand movement has served as an impetus to the development of brain-controlled prostheses for the movement-impaired population. Prior to the advent of brain-controlled prostheses, several seminal discoveries laid a foundation with arguably the most momentous discovery being that of a population vector code for the direction of hand movement in three-dimensions (Georgopoulos et al. 1986; Kettner et al. 1988). At the beginning of this century, researchers launched the field of brain-controlled neuromotor prostheses with the application of the population vector algorithm

as well as other methods to extract control signals related to hand movement from neural data (Schwartz et al. 2001). Researchers have demonstrated the ability to decode hand kinematics at the microscale from neuronal signals acquired with microwires or microelectrode arrays seated into small patches of sensorimotor cortical tissue and to use this information to drive a cursor or robotic arm (Wessberg et al. 2000; Serruya et al. 2002; Taylor et al. 2002; Hochberg et al. 2006; Santhanam et al. 2006; Truccolo et al. 2008; Velliste et al. 2008; Mulliken et al. 2008). Other intracranial studies have analyzed neural data at the mesoscale with coarser spatial resolution but wider spatial extent from local field potential (LFP) recordings. For example, hand movement direction and two-dimensional trajectories have been decoded from LFPs (Mehring et al. 2003; Mehring et al. 2004; Leuthardt et al. 2004; Rickert et al. 2005; Scherberger et al. 2005; Schalk et al. 2007; Pistohl et al. 2008; Sanchez et al. 2008).

In the late 1990s, pioneering work on the macroscale began to relate scalp potentials acquired noninvasively to hand movement (Kelso et al. 1998; O'Suilleabhain et al. 1999). Some recent noninvasive studies have demonstrated the presence of a macroscale network that carries the neural code for detailed hand movement. For instance, hand movement direction has been decoded from electroencephalography (EEG) and MEG data (Hammon et al. 2008; Waldert et al. 2008), and hand position and velocity have been decoded from MEG data collected during continuous joystick and trackball movements (Georgopoulos et al. 2005; Jerbi et al. 2007). However, with the exception of Hammon et al., these noninvasive studies have constrained subjects to small finger and wrist movements as opposed to multijoint drawing or reaching movements. Also, most

importantly, the tasks employed for noninvasive decoding of hand position and velocity have not incorporated discrete center-out movements.

To examine our hypothesis that hand kinematics of *natural*, *multijoint*, *center-out* movements are decodable from noninvasive neural signals, we aimed to continuously decode hand velocity from MEG data collected during a two-dimensional drawing task. Currently only invasive studies have continuously decoded hand velocity during discrete center-out movements. Since MEG coupled with our decoding method facilitates the ability to examine sensor involvement on a macroscale with high temporal resolution, we also sought to create snapshots of sensor importance in a network covering multiple brain regions across time during adaptation to a hand-cursor rotation. Furthermore, we aimed to examine the importance of estimated current sources in the network using sLORETA to determine whether they corroborated non-decoding visuomotor adaptation studies that employed other imaging modalities like EEG (Contreras-Vidal and Kerick 2004), positron emission tomography (PET) (Inoue et al. 2000; Ghilardi et al. 2000; Krakauer et al. 2004), and functional magnetic resonance imaging (fMRI) (Graydon et al. 2005; Seidler et al. 2006).

Materials and methods

Experimental procedure and data collection

The Institutional Review Board of the University of Maryland at College Park approved the following experimental procedure. After giving informed consent, five healthy, right-

handed subjects drew center-out lines with an optic pen on a glass panel positioned in front of them while they lay supine with their heads in an MEG recording dewar located inside a magnetically shielded room in the Kanazawa Institute of Technology (KIT)-Maryland MEG laboratory at the University of Maryland (Fig. 1.1A). Cushions were positioned in the dewar and under the right elbow to minimize movement of the head and upper limb respectively. The distance between the glass panel and each subject's head was adjusted for comfort (approximately 35 cm from nose tip to the center of the panel). A black curtain occluded the subjects' vision of their hands while visual feedback was provided on a screen located in front of them that displayed the position of the pen tip as a cursor. Subjects were instructed to position the pen tip in a circle (0.5 cm diameter) located in the middle of the screen, wait for one of four circle targets (0.5 cm diameter) to appear in the corner of the screen at 45, 135, 225, or 315°, wait for the target to change color, and then draw a straight line to the target as fast as possible. The inter-trial delay was randomized between 2 and 2.5 s. Working space dimensions were a 10×10 cm virtual square. After 40 trials (pre-exposure), the cursor was rotated 60° counterclockwise (exposure). The exposure phase consisted of 240 trials with the early-exposure phase composed of the first 40 trials and the late-exposure phase composed of the last 40 trials. After the exposure phase, the original orientation of the cursor was restored, and 20 more trials were collected and labeled as the post-exposure phase. The number of trials analyzed in the pre-exposure phase was reduced from 40 to 36 because the behavioral performance during several initial trials of some subjects was poor due to lack of familiarization with the task. To maintain consistency, the number of trials analyzed in the early- and late-exposure phases was also reduced from 40 to 36.

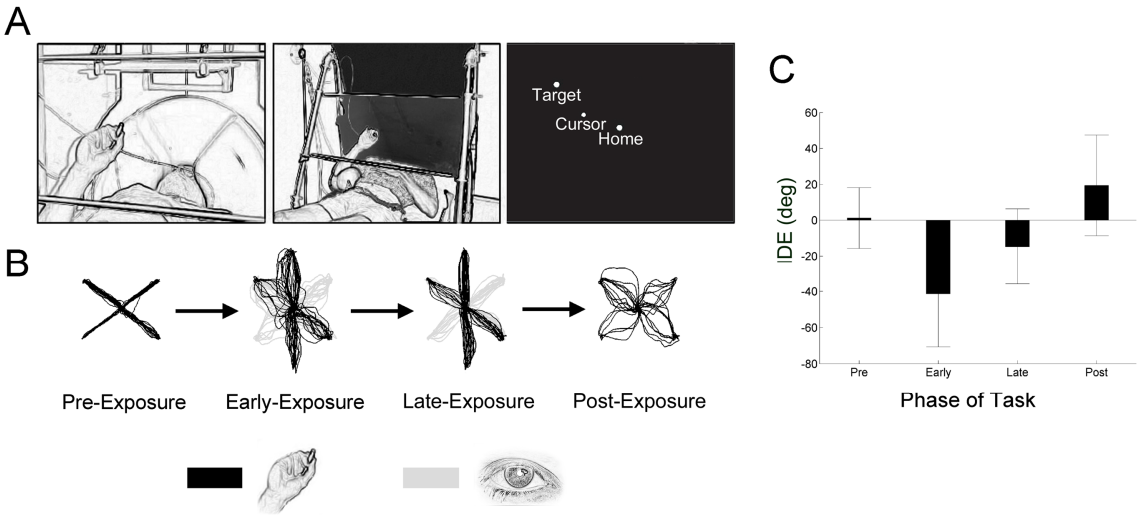

Fig. 1.1. Center-out drawing experimental setup and kinematics. (A) In the first and second panels, a subject is shown lying with his head inside the MEG recording dewar and drawing with an optic pen on a sheet of glass. A black curtain used to occlude vision of the upper limbs is additionally shown in the second panel. The third panel illustrates the subject's view of the computer screen where visual feedback of the pen position (cursor), center location (home), and peripheral targets was displayed. (B) The superimposed pen (black) and cursor (gray) paths for one representative subject confirmed the occurrence of adaptation. Dissociation between the pen (hand) and cursor (eye) movements due to hand-cursor rotation was evident. (C) The mean ± SD of the IDE calculated across subjects for each phase of the task further confirmed adaptation.

A video camera sampled the movement of the pen tip at 60 Hz, and whole-head MEG data were acquired from 157 channels at a sampling rate of 1 kHz. The MEG system used coaxial type first-order gradiometers with a magnetic field resolution of 4 ft/Hz$^{1/2}$ or 0.8 (ft/cm)/Hz$^{1/2}$ in the white noise region. On-line, electronic circuits band-pass and notch-filtered the MEG data from 1–100 Hz and 60 Hz respectively.

Adaptation confirmation

To quantitatively confirm the occurrence of adaptation, the mean initial directional error (IDE) was calculated across subjects for each phase of the task. A vector from the center location of the screen (home) to the position of the pen at 80 ms after the pen completely left the center circle determined the initial direction of the planned movement trajectory. The IDE was calculated as the angular difference between this vector and a vector extending from the home location to the target. Four separate *t*-tests were performed between the IDE in pre-exposure and zero, IDE in pre-exposure and early-exposure, IDE in pre-exposure and late-exposure, and IDE in pre-exposure and post-exposure.

Signal pre-processing

Data from each MEG sensor were first standardized according to Eq. (1.1):

$$S_n[t] = \frac{s_n[t] - \bar{s}_n}{SD_{s_n}} \quad \text{for all } n \text{ from 1 to } N \tag{1.1}$$

where $S_n[t]$ and $s_n[t]$ are respectively the standardized and measured magnetic field strength of sensor n at time t, $\bar{s}_n$ and SD_{sn} are the mean and standard deviation of s_n respectively, and N is the number of sensors. The kinematic data were resampled from 60 Hz to 1 kHz by using a polyphase filter with a factor of $^5/_3$. For computational efficiency, the MEG and kinematic data were then decimated from 1 kHz to 100 Hz by applying a low-pass anti-aliasing filter with a cutoff frequency of 40 Hz and then downsampling. The best decoding results were obtained when both the MEG and kinematic data were subsequently filtered with a zero-phase, fourth-order, low-pass

Butterworth filter with a cutoff frequency of 15 Hz. The data for each phase of the task were pre-processed separately.

Decoding model

In the subsequent analyses, we only considered hand velocity based on our previous work that revealed better decoding of hand velocity than hand position from MEG signals (Bradberry et al. 2008). To continuously decode hand velocity from the MEG signals, a linear decoding model was used (Fig. 1.2) (Georgopoulos et al. 2005):

$$x[t] - x[t-1] = \sum_{n=1}^{N} \sum_{k=0}^{L} b_{nkx} S_n[t-k] \tag{1.2}$$

$$y[t] - y[t-1] = \sum_{n=1}^{N} \sum_{k=0}^{L} b_{nky} S_n[t-k] \tag{1.3}$$

where $x[t]$ and $y[t]$ are the horizontal and vertical position of the pen at time sample t respectively, N is the number of MEG sensors, L is the number of time lags, $S_n[t-k]$ is the magnetic field strength measured at MEG sensor n at time lag k, and the b variables are coefficients obtained through multiple regression. By varying the number of lags and sensors independently in a step-wise fashion, the optimal number of lags ($L = 20$, corresponding to 200 ms) and the best sensors ($N = 62$; from central and posterior scalp regions) were determined experimentally. The data for each phase of the task were decoded separately.

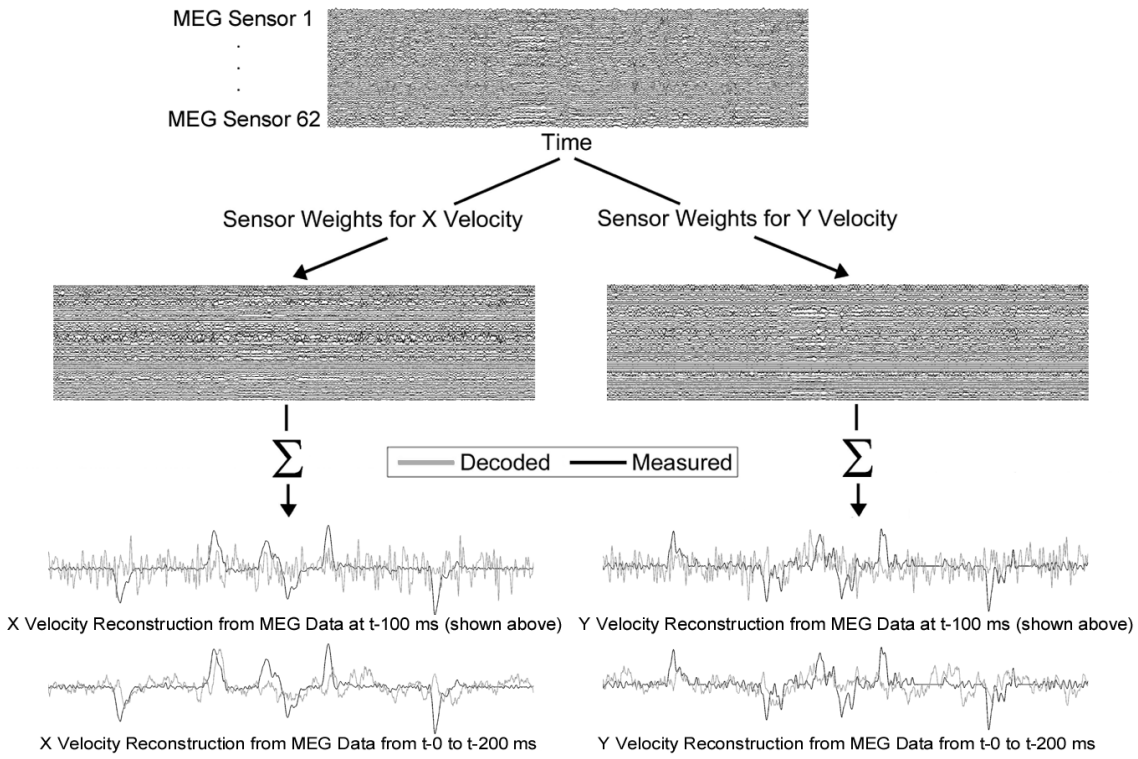

Fig. 1.2. Didactic model of the linear decoding method. The top raster plot contains time series of 62 MEG sensors extracted 100 ms prior to the current velocity sample of interest. Through multiple linear regression, sensor weights were computed separately for *x* and *y* velocity that transformed the top raster plot to the lower left and right raster plots. The transformed time series of the sensors were then summed to produce the reconstructed velocity profiles (gray) that overlay the measured velocity profiles (black). The upper velocity profiles are associated with the MEG data shown in the example (100 ms prior to the current velocity sample of interest) and the lower ones with MEG data from 0 to 200 ms prior to the current velocity sample of interest.

Assessment of decoding accuracy

M-fold cross-validation was used to assess the decoding accuracy. In this procedure, the data were divided into *m* parts (each with approximately 12 s of continuous data, or four trials), $m - 1$ parts were used for training, and the remaining part was used for testing. The procedure was considered complete when each of the *m* combinations of training and testing data were exhausted, and the mean CC between measured and decoded hand velocity was computed across folds. Prior to computing the CC, the kinematic signals were smoothed with a fourth-order, low-pass Butterworth filter with a cutoff frequency of 0.6 Hz. Cross-validation was executed with $m = 9$ for all phases of the task except for post-exposure where $m = 5$. For Fig. 1.3B, standardized velocity profiles were computed with Eq. (1.1) with s_n replaced by a velocity profile.

Sensor sensitivity curves

A curve depicting the relationship between decoding accuracy and the number of sensors was computed for the *x* and *y* dimensions of hand velocity for each subject for each phase of the task. A similar method to examine this relationship has been used to analyze neuronal recordings (Sanchez et al. 2004). First, for each subject and each phase of the task, each sensor was assigned a rank according to Eq. (1.4):

$$R_n = \frac{1}{M(L+1)} \sum_{k=0}^{L} \sum_{m=1}^{M} \sqrt{b_{mnkx}{}^2 + b_{mnky}{}^2} \quad \text{for all } n \text{ from 1 to } N \tag{1.4}$$

where R_n is the rank of sensor *n* and *M* is the number of folds of the cross-validation procedure. Second, the decoding model was iteratively executed with only the highest-ranked sensor, the four highest-ranked sensors, the seven highest-ranked sensors, etc.

until all sensors were used. For each phase of the task, the mean ± SD of the CCs computed across subjects was plotted against the number of sensors. Finally, each plot was fitted to a double-exponential curve, and the coefficient of determination, R^2, was calculated as a measure of the goodness of fit.

Scalp maps of sensor contributions

To graphically assess the relative contributions of scalp regions to the reconstruction of hand velocity, the across-subject means of the *b* (from Eqs. (1.2) and (1.3)) vector magnitude were projected onto a time series (− 200 to 0 ms in increments of 10 ms) of scalp maps for each phase of the task. These spatial renderings of sensor contributions were produced by the topoplot function of EEGLAB version 6.01b, an open-source MATLAB toolbox for electrophysiological data processing (Delorme and Makeig 2004, http://sccn.ucsd.edu/eeglab/), that performs biharmonic spline interpolation of the sensor values before plotting them (Sandwell 1987). To examine which time lags were the most important for decoding, for each scalp map, the percentage of reconstruction contribution for a phase of the task was computed as

$$\%T_i = 100\% \times \frac{\sum_{n=1}^{N} \sqrt{{b_{nix}}^2 + {b_{niy}}^2}}{\sum_{k=0}^{L} \sum_{n=1}^{N} \sqrt{{b_{nkx}}^2 + {b_{nky}}^2}} \quad \text{for all } i \text{ from 0 to } L \tag{1.5}$$

where $\%T_i$ is the percentage of reconstruction contribution for a scalp map at time lag *i*.

Comparison of scalp maps across adaptation

Right-tailed, paired *t*-tests determined statistically significant ($p < 0.05$) changes in sensor contributions between phases of the task. Three contrasts between the scalp maps were computed for increases from baseline (pre-exposure): early-exposure – pre-exposure, late-exposure – pre-exposure, and post-exposure – pre-exposure; and three contrasts were computed for decreases from baseline: pre-exposure – early-exposure, pre-exposure – late-exposure, and pre-exposure – post-exposure. The resultant *t* scores were converted to *z* scores and then rendered onto scalp maps with the topoplot function of EEGLAB (Delorme and Makeig 2004) with increases and decreases represented with hot and cool colors respectively.

Cortical source localization

To better estimate the cortical sources of hand velocity encoding in each phase of the task, we used standardized low-resolution brain electromagnetic tomography (sLORETA) software version 20081104 (Pascual-Marqui 2002, http://www.uzh.ch/keyinst/loreta.htm). sLORETA computes instantaneous, 3-D linear, distributed and discrete solutions for the MEG/EEG inverse problem, which compare well with respect to linear inverse algorithms like minimum norm solution, weighted minimum norm solution, and weighted resolution optimization (Pascual-Marqui 2002). These solutions are computed within a three-shell spherical head model that uses a lead field computed with a boundary element method applied to the MNI52 template (Fuchs et al. 2002). The head model includes scalp, skull, and brain compartments. The brain compartment is restricted to the cortical matter of a head model co-registered to the

Talairach brain atlas (Talairach and Tournoux 1988). This compartment includes 6239 voxels at 5 mm resolution with each voxel containing a current dipole representing the integrated activity within the corresponding spatial vicinity. The sensor coordinates of the MEG helmet that were entered into sLORETA had been previously measured in the KIT-Maryland MEG laboratory.

To identify sources that were sensitive to velocity encoding, we found the sources that best correlated with the most meaningful sensors from the decoding analysis using the following method. Pre-processed MEG signals from all 157 channels for each subject and each phase of the task were fed to sLORETA to estimate current sources. These MEG signals had been pre-processed in the same manner as for decoding: standardized, downsampled, and low-pass filtered. From the scalp map with the highest percentage of reconstruction contribution (− 100 ms), the fifteen sensor weights possessing the highest values were selected. The CCs were then computed between the squared time series from the fifteen sensors with the 6239 time series from the sLORETA solutions and averaged across subjects. Each CC was multiplied by the magnitude of the regression weight *b* (from Eqs. (1.2) and (1.3)) vector of the sensor in the correlation analysis. The reason that fifteen sensors were chosen for the correlation analysis was because of the observation that the sensor sensitivity curves began to plateau around fifteen sensors (Fig. 1.4). Next the highest 5% of the CCs (weighted by *b*) were set to the value one, and the rest of the CCs were set to zero. Finally these binary-thresholded CCs were plotted onto an axial slice of the brain (z = 55 mm) from the Colin27 volume (Holmes et al. 1998), the MRI

template that best illustrated our regions of interest. All reported coordinates of regions of interest are in Talairach space.

Ancillary analysis: decoding from artifact-cleaned MEG data

Unintended contributions of eye movements to the decoding of hand movement is a potential confound in all MEG, EEG, and ECoG studies, including our study. We did not experimentally control eye movements; however, we performed an ancillary analysis. The following procedure was separately performed on data from each phase of the task. The continuous kinematic and MEG data for a phase of the task were split into discrete single trials of center-out drawing. Ocular, muscular, and cardiac artifacts were removed by using independent component analysis (ICA) to extract independent components (ICs) and then comparing the ICs to templates of known artifacts for the purpose of categorization and subsequent removal of the artifacts (Rong and Contreras-Vidal 2006). The MEG data were downsampled to 60 Hz to match the sampling rate of the kinematic data and then standardized (Eq. (1.1)). The same central and posterior scalp areas were used in the decoding model ($N = 62$), and no time lags ($L = 0$) were used because of the discontinuities due to concatenation. Cross-validation with half of the data as testing and the other half as training was performed for 500 runs with the single trials shuffled and concatenated before each run. The mean and SD of the CCs for the 500 runs were calculated for each subject during each phase of the task.

Results

Hand kinematics confirmed adaptation

During early-exposure to the cursor rotation, we observed curved hand paths due to the subjects' effort to counteract the imposed rotation (Fig. 1.1B). Hand paths became straighter in late-exposure as subjects adapted to the novel environment. In post-exposure, after-effects, which consisted of hand paths curved in the opposite direction from those in early-exposure, indicated that adaptation had occurred. We also confirmed the occurrence of adaptation quantitatively by computing the mean IDE across subjects for each phase of the task and comparing it between phases (Fig. 1.1C). The IDE was not significantly different from zero in pre-exposure (two-tailed *t*-test; $p = 0.34$). The IDE increased in early-exposure relative to pre-exposure, decreased in late-exposure relative to early-exposure, and increased again in post-exposure relative to pre-exposure (one-tailed, paired *t*-tests, $p < 0.001$).

MEG signals contained decodable hand velocity information

We employed a linear decoding model (Eqs. (1.2) and (1.3)) to reconstruct the horizontal (x) and vertical (y) velocity components of hand movement from the activity of the MEG sensors (Fig. 1.2). The mean CC of x velocity decreased during each consecutive phase of the adaptation task (Fig. 1.3A). Interestingly the mean CC of y velocity increased until post-exposure at which point it drastically decreased. In terms of individual subjects, the mean CCs ranged from 0.23 to 0.56 (Table 1.1), and examples of smoothed, reconstructed hand velocity profiles matched the measured velocity profiles well (Fig. 1.3B).

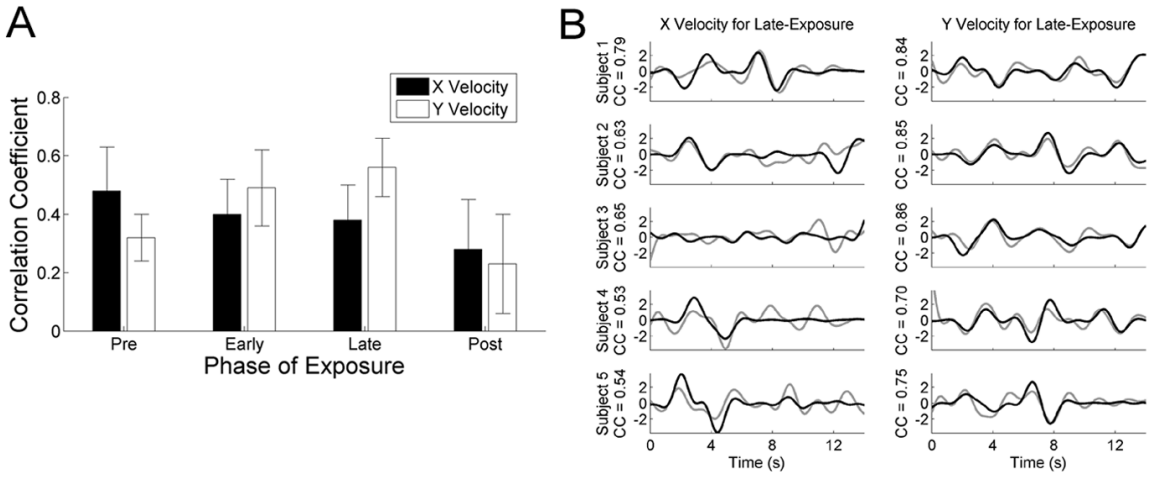

Fig. 1.3. Decoding accuracy for hand velocity. (A) The across-subject mean ± SD of the CCs between measured and decoded hand velocity profiles is plotted separately for *x* (horizontal, black) and *y* (vertical, white) velocity for each phase of the task. (B) Examples of smoothed and standardized measured (black) and decoded (gray) hand velocity profiles for late-exposure exhibited high decoding accuracy. The left and right columns contain *x* and *y* velocity profiles respectively. Each row contains data for a single subject, and the CC between the measured and decoded velocity is listed to the left of each plot.

Table 1.1. Mean and SD (in parentheses) of CCs for each subject during each phase of the visuomotor adaptation task.

	Pre		**Early**		**Late**		**Post**	
	X Vel	**Y Vel**	**X Vel**	**Y Vel**	**X Vel**	**Y Vel**	**X Vel**	**Y Vel**
Subject 1	0.64 (0.09)	0.47 (0.16)	0.44 (0.11)	0.62 (0.13)	0.53 (0.13)	0.73 (0.12)	0.10 (0.21)	-0.02 (0.13)
Subject 2	0.45 (0.16)	0.29 (0.14)	0.56 (0.10)	0.45 (0.11)	0.40 (0.18)	0.52 (0.21)	0.10 (0.07)	0.37 (0.13)
Subject 3	0.48 (0.14)	0.23 (0.21)	0.46 (0.16)	0.53 (0.18)	0.49 (0.12)	0.63 (0.24)	0.42 (0.16)	0.26 (0.14)
Subject 4	0.60 (0.08)	0.33 (0.22)	0.21 (0.20)	0.23 (0.11)	0.21 (0.18)	0.44 (0.15)	0.55 (0.07)	0.46 (0.13)
Subject 5	0.17 (0.21)	0.26 (0.30)	0.26 (0.13)	0.58 (0.14)	0.24 (0.15)	0.47 (0.22)	0.17 (0.32)	0.02 (0.13)
Grand Mean	0.48 (0.15)	0.32 (0.08)	0.40 (0.12)	0.49 (0.13)	0.38 (0.12)	0.56 (0.10)	0.28 (0.17)	0.23 (0.17)

Number of sensors and decoding accuracy were exponentially related

The linear decoding model produced one weight per sensor per time lag; therefore, the importance of the contribution of a sensor to the decoding process at a particular time lag could be considered the vector magnitude of its regression weights at that time lag. We ranked the sensors and reran the decoding procedure with the most important sensor, the four most important sensors, the seven most important sensors, etc. until all sensors were used. These sensor sensitivity curves of mean CC vs. the number of sensors fit a double-exponential function well (R^2 = 0.95–1.00) (Fig. 1.4). For all phases of the task, the curves peaked then plateaued, or nearly plateaued, near 15 sensors.

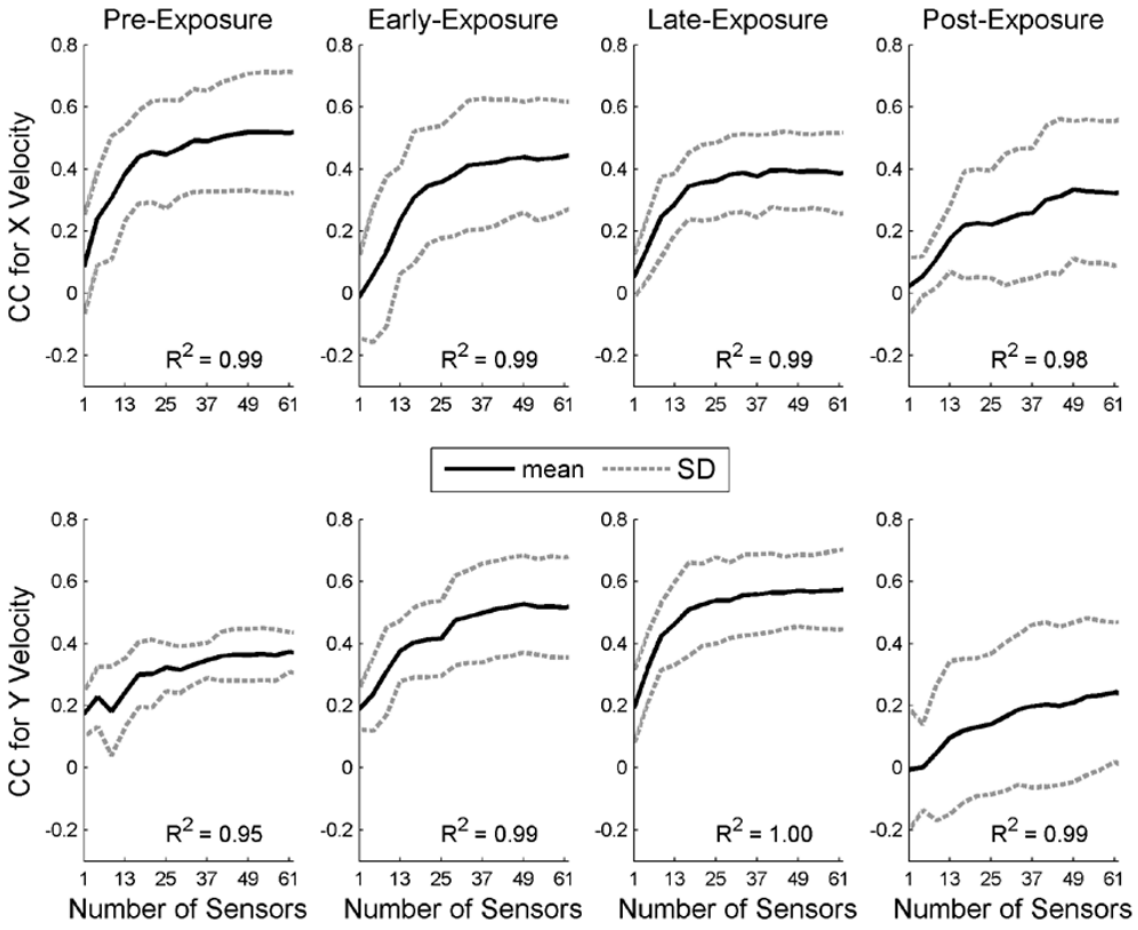

Fig. 1.4. Decoding accuracy vs. number of sensors. The top and bottom rows contain plots of mean (black) ± SD (gray) of the CCs across subjects vs. the number of sensors for *x* and *y* velocity respectively. Columns organize the plots by phase of the task. R^2 values between the mean CC curve and a fitted double-exponential curve are displayed at the bottom of each plot.

A macroscale sensorimotor network encoded hand velocity

To graphically assess the relative contributions of scalp regions to the reconstruction of hand velocity, we projected the across-subject means of the vector magnitudes of the sensor weights onto a time series (− 200 to 0 ms in increments of 10 ms) of scalp maps for each phase of the adaptation task. The scalp maps for each phase of the task resembled each other, so only those for pre-exposure are shown (Fig. 1.5A). A network of sensors over central and posterior scalp areas contributed to decoding hand velocity with a salient member of the network over the contralateral motor area. Although the scalp maps of the different phases appeared similar upon visual inspection, we investigated the presence of statistically significant increases and decreases in early-, late-, and post-exposure relative to baseline (pre-exposure). We observed notable focal differences between phases of the task in scalp areas over mediolateral premotor and posterior parietal cortices in particular (Fig. 1.5B). To better estimate the cortical sources that gave rise to the scalp maps at − 100 ms (the highest percentage of reconstruction contribution), we correlated the fifteen best sensors with the sources estimated by sLORETA. After weighting the CCs by the vector magnitudes of the sensor weights, the top 5% were binary-thresholded and plotted on an axial slice (Fig. 1.5C). In all phases of

the task, the contralateral precentral gyrus (PrG) and postcentral gyrus (PoG) and the ipsilateral superior parietal lobule (SPL) and precuneus (PCu) encoded for hand velocity. The contralateral inferior parietal lobule (IPL) and ipsilateral medial frontal gyrus, containing the supplementary motor area (SMA), additionally encoded for hand velocity in all phases except pre-exposure. Finally the lateral premotor cortex of the bilateral middle frontal gyrus (MFG) and ipsilateral superior frontal gyrus (SFG) were involved in hand velocity encoding only in early- and post-exposure.

Ancillary analysis: similar decoding resulted from artifact-cleaned MEG data

Regarding the ancillary analysis of artifact-cleaned MEG data, although there was a notable drop in decoding accuracy for *y* velocity in pre- and post-exposure, there was no statistically significant difference in the resultant mean CCs of the subjects for any phase of the task (two-tailed, paired *t*-test; $p > 0.05$) (Table 1.2).

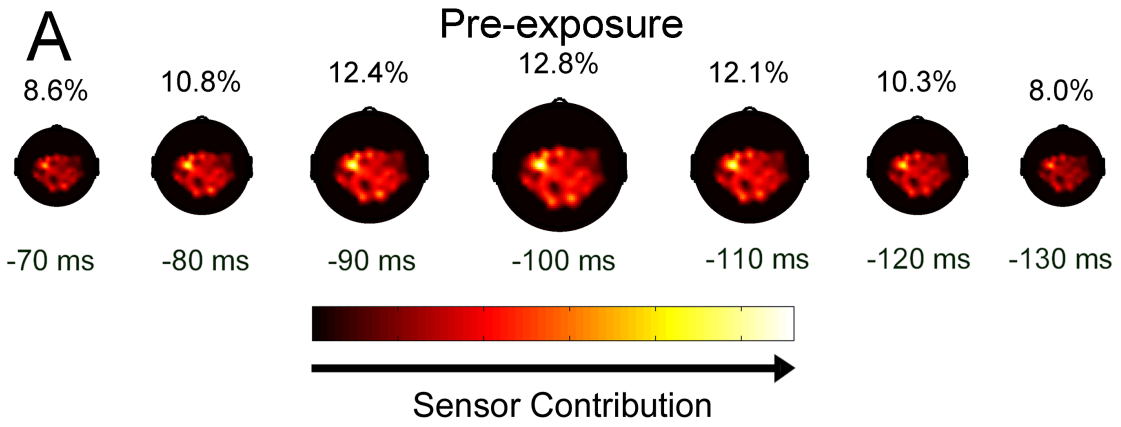
A
Pre-exposure
8.6%
10.8%
12.4%
12.8%
12.1%
10.3%
8.0%
-70 ms
-80 ms
-90 ms
-100 ms
-110 ms
-120 ms
-130 ms
Sensor Contribution

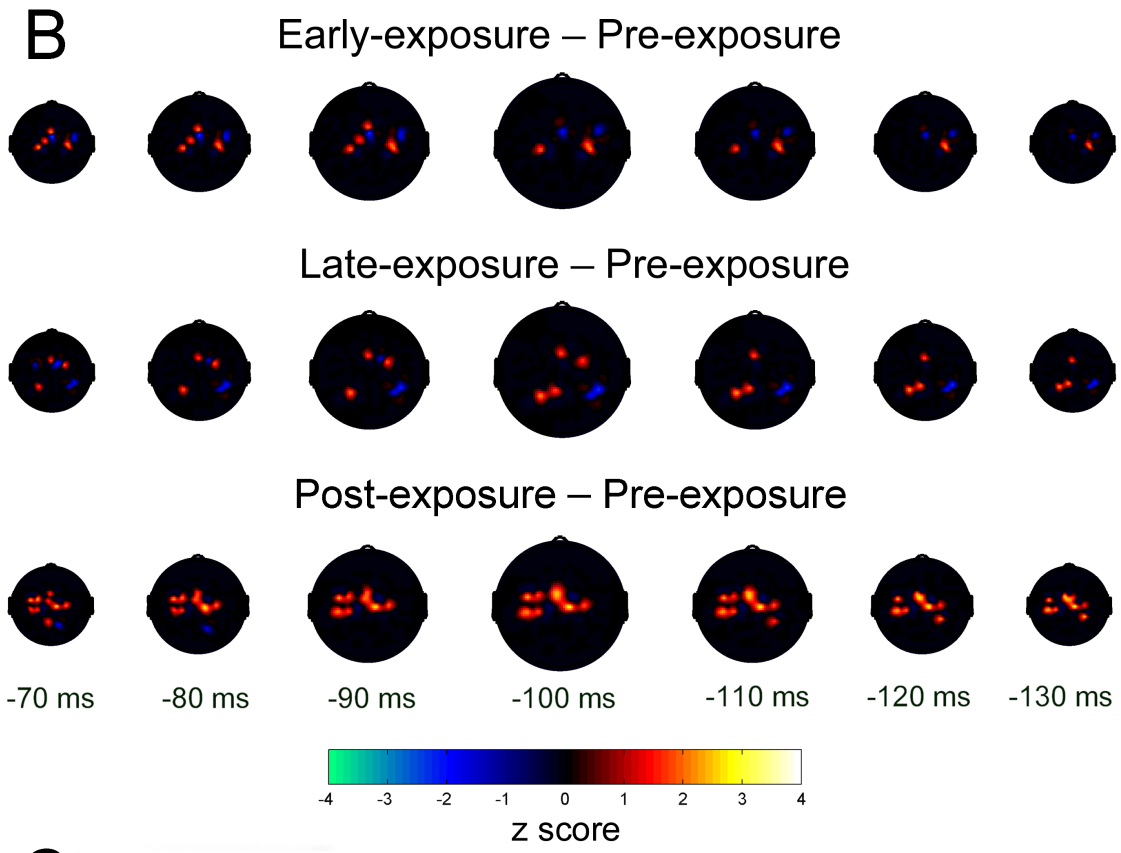
B
Early-exposure – Pre-exposure
Late-exposure – Pre-exposure
Post-exposure – Pre-exposure
-70 ms
-80 ms
-90 ms
-100 ms
-110 ms
-120 ms
-130 ms
-4
-3
-2
-1
0
1
2
3
4
z score

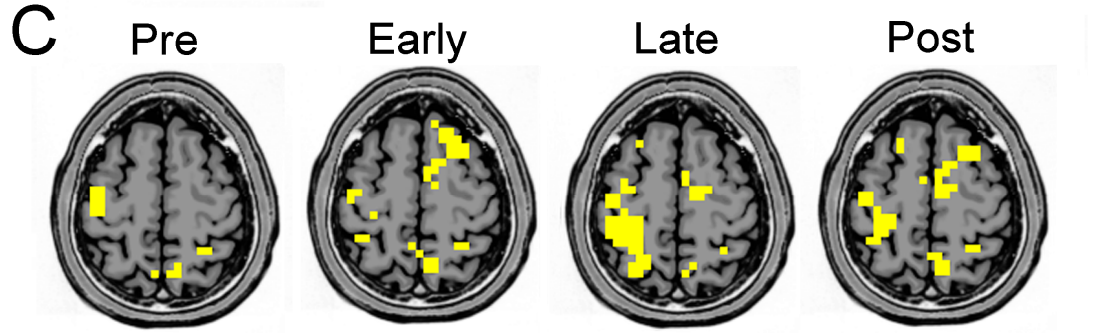
C
Pre
Early
Late
Post

Fig. 1.5. Sensorimotor networks associated with hand velocity during visuomotor adaptation. (A) The mean vector magnitudes of the sensor weights from the linear decoding model revealed the importance of neural regions when interpolated and projected onto a time series (− 200 to 0 ms in increments of 10 ms) of scalp maps for the pre-exposure phase (other phases were similar). Light and dark colors represent high and low contributors respectively. The highest sensor weighting of the MEG signals led the velocity output by 100 ms, so the display of scalp maps are centered around − 100 ms. The percentage of reconstruction contribution (%*T*) is displayed above each scalp map. Due to space limitations, only seven of the twenty-one scalp maps are shown. (B) The rows respectively contain the *z* scores of differences between early- and pre-exposure, late- and pre-exposure, and post- and pre-exposure. Increased (+) and decreased (−) contributions of sensors are mapped to hot and cool colors respectively. (C) The estimated cortical sources involved in hand velocity encoding during the task were represented on an axial slice from an MRI template ($z = 55$). The sources and their Talairach coordinates (*x, y, z*) were the PrG (− 41, − 11, 55), PoG (− 45, − 17, 55), SPL (30, − 46, 55), PCu (3, − 61, 55), IPL (− 41, − 41, 55), SMA (5, − 2, 55), MFG (19, 18, 55 and − 24, 20, 55), and SFG (19, 12, 55).

Table 1.2. Mean and SD (in parentheses) of the CCs for each subject during each phase of the visuomotor adaptation task for the decoding procedure with artifact-cleaned MEG data.

	Pre		**Early**		**Late**		**Post**	
	X Vel	**Y Vel**	**X Vel**	**Y Vel**	**X Vel**	**Y Vel**	**X Vel**	**Y Vel**
Subject 1	0.44 (0.09)	0.46 (0.10)	0.52 (0.07)	0.37 (0.09)	0.46 (0.12)	0.66 (0.08)	0.44 (0.14)	0.09 (0.16)
Subject 2	0.21 (0.09)	-0.17 (0.10)	0.18 (0.11)	0.13 (0.09)	0.37 (0.07)	0.31 (0.09)	0.02 (0.16)	0.13 (0.18)
Subject 3	0.42 (0.08)	0.05 (0.13)	0.75 (0.05)	0.54 (0.06)	0.66 (0.07)	0.63 (0.05)	0.63 (0.10)	0.15 (0.20)
Subject 4	0.70 (0.05)	0.04 (0.15)	0.41 (0.09)	0.24 (0.10)	0.47 (0.08)	0.54 (0.06)	0.44 (0.12)	-0.02 (0.16)
Subject 5	0.55 (0.10)	0.26 (0.17)	0.32 (0.09)	0.36 (0.11)	0.38 (0.15)	0.48 (0.13)	0.20 (0.20)	0.20 (0.22)
Grand Mean	0.46 (0.16)	0.13 (0.21)	0.44 (0.19)	0.33 (0.14)	0.47 (0.10)	0.52 (0.12)	0.35 (0.21)	0.11 (0.07)

Discussion

Our results demonstrate that we can continuously decode information about hand velocity from natural, multijoint, center-out movements from MEG signals collected during a drawing task that requires visuomotor adaptation to a hand-cursor rotation. With the systematic addition of sensors to the decoding model, the decoding accuracy exponentially increases before reaching a plateau. Additionally, a macroscale sensorimotor network composed of central and posterior scalp regions encodes for hand velocity in all phases of adaptation, and the differences in MEG sensor importance between phases capture the evolution of cortical involvement during adaptation. Furthermore, localization of cortical sources permits a more detailed investigation into the cortical regions that encode for hand velocity in different adaptation phases.

Hand velocity information is represented on multiple spatial scales

Researchers have firmly established the existence of a population code for hand position and velocity at the microscale level via neuronal recordings (Georgopoulos et al. 1986; Kettner et al. 1988; van Hemmen and Schwartz 2008). Recently, some electrocorticography (ECoG) studies demonstrated that a population code for these kinematic parameters also exists on a mesoscale (Schalk et al. 2007; Pistohl et al. 2008; Sanchez et al. 2008). The most striking result of our study is that a sensorimotor network on a larger spatial scale encodes hand kinematics during natural, multijoint center-out movements, and, furthermore, does so during adaptation to a screen cursor-hand rotation. In sensor space, this network spans central and posterior sensor areas. Each MEG sensor

reflects the contributions of millions of neurons, but yet, we can still decode information about hand velocity.

Further regarding spatial scale, we asked whether a denser sampling of the scalp space could improve decoding accuracy. Since the curves of mean CC vs. the number of sensors reveal there to be an optimal, or near optimal, number of sensors less than 62 for all phases of the task (Fig. 1.4), we conclude that the addition of more sensors would not substantially improve the decoding accuracy. The decreased mean decoding accuracy and increased SD of the CCs during post-exposure is likely due to the relatively small amount of data collected and analyzed during this phase of the task. The overall increased mean decoding accuracy of *y* velocity during adaptation was potentially due to the fact that, during exposure, the 60-degree rotation had a greater affect on hand movement in the *y* direction than the *x* direction, and thus may have recruited more neural resources to handle the *y* direction (Contreras-Vidal and Kerick 2004).

Several interesting pieces of evidence serve to validate the interpretation of our decoding results. First, the greatest sensor contributions across time lags occur at 100 ms prior to the current kinematic sample under reconstruction for all phases of the task (Fig. 1.5A). Given that prior research has established approximately 100 ms of neural data in the past to be important for planning the current movement (Mehring et al. 2004; Paninski et al. 2003), this finding is not unexpected. In our previous report leading up to this study (Bradberry et al. 2008), we discovered that hand velocity was better decoded than position (post-publication analysis: two-tailed, paired *t*-test; $p < 0.0001$). This is another

confirmatory finding, given that the motor cortex represents velocity better than position as has been demonstrated, in particular, by studies aimed at decoding kinematic parameters for neuroprosthetic control (Schwartz et al. 2001). Furthermore, the salient region of high activation over the left motor area is expected since subjects drew with their right hands.

Regional comparison to non-decoding studies of visuomotor adaptation

In sensor space, across adaptation we find significant contributions to hand velocity decoding over the mediolateral premotor and posterior parietal scalp areas with respect to pre-exposure (Fig. 1.5B). Previous studies demonstrated that the parietal and premotor cortices are involved in a visuomotor network for reaching (Wise et al. 1997; Burnod et al. 1999), and an EEG study of visuomotor adaptation reported fronto-parietal shifts (Contreras-Vidal and Kerick 2004). To speak more specifically about the cortical areas involved with visuomotor adaptation and encoding of hand kinematics, we performed source localization (Fig. 1.5C). Multiple similarities exist between the cortical regions found in our study and those of fMRI and PET studies of visuomotor adaptation. The left PrG, PoG, and IPL have been shown to be involved during visuomotor adaptation to a rotation of visual feedback by a fMRI studies by Graydon et al. (2005) and Seidler et al. (2006). In PET studies, the right SPL has been observed to increase in activation during visuomotor adaptation tasks by Inoue et al. (2000), Ghilardi et al. (2000), and Krakauer et al. (2004). Inoue et al., Krakauer et al., and Seidler et al. have also revealed an increase in activation of SMA/preSMA during visuomotor adaptation. Finally the MFG and SFG

(lateral premotor cortex) have been shown to be active in visuomotor adaptation by Inoue et al. and Seidler et al.

Regional comparison to other decoding studies

Regarding decoding of hand kinematics, the common involvement across tasks of the PrG, PoG, SPL, and PCu implies that these areas form the core for hand velocity encoding in familiar and unfamiliar environments while the SMA, lateral premotor cortex, and IPL encode for hand velocity only during adaptation. Decoding of hand kinematics has been reported for PrG and PoG at a microscale (Georgopoulos et al. 1986; Moran and Schwartz 1999; Wessberg et al. 2000; Serruya et al. 2002; Schwartz et al. 2004), mesoscale (Schalk et al. 2007, Pistohl et al. 2008; Sanchez et al. 2008), and macroscale (Jerbi et al. 2007). This decoding role has also been ascribed to the SPL at the microscale (Averbeck et al. 2005; Averbeck et al. 2009; Mulliken et al. 2008) and macroscale (Jerbi et al. 2007). The SMA/preSMA, lateral premotor cortex, and IPL have also been observed to encode movement kinematics (Moran and Schwartz 1999; Schwartz et al. 2004; Jerbi et al. 2007; Tankus et al. 2009). On a slightly different note, a PET study that examined the control of movement velocity, discovered the involvement of left PrG, left PoG, right SPL, and mediolateral premotor cortex (Turner et al. 1998). To our knowledge, we are the first to report that the PCu plays a role in the encoding of detailed hand kinematics.

Could eye movements have inadvertently aided hand velocity decoding?

Unintended contributions of eye movements to the decoding of hand movement is a potential confound in all MEG, EEG, and ECoG studies, including our study. We do not experimentally control eye movements; however, our ancillary analysis, which removes ocular activity with an ICA-based method, demonstrates that ocular movements do not significantly affect decoding (Table 1.2).

Potential application to neuromotor prosthetic control

Most studies involving noninvasive BCI systems have focused on 1) the classification of mental tasks to form a low bandwidth communication channel (Pfurtscheller et al. 2006; Mellinger et al. 2007) or 2) continuous control of a cursor by subjects who, through relatively lengthy biofeedback training, learn to modulate the power of one or more frequency bands of neural signals to control one or more dimensions of cursor movement (Wolpaw and McFarland 2004; McFarland et al. 2008). The lack of focus on decoding detailed kinematics of natural hand movements could be partly due to the unfounded presumption that this information cannot be decoded from noninvasive signals recorded from the scalp (Lebedev and Nicolelis 2006). Despite this presumption, there exist several important exceptions to the lack of noninvasive studies aimed at developing decoding methods for controlling neuromotor prostheses. One study has decoded continuous joystick coordinates from MEG signals acquired during continuous pentagon drawing in the absence of visual feedback of movement (Georgopoulos et al, 2005), and another study has decoded information regarding hand tangential velocity from MEG signals acquired during trackball movements in two dimensions (Jerbi et al. 2007). Our

study primarily differs from the two aforementioned studies in that we decode continuous hand velocity from *multijoint* movements during a *center-out* drawing task that requires adaptation to a novel *screen-cursor rotation*. The center-out nature of our task is meaningful because it allows comparison to invasive decoding studies for neuromotor prostheses and emphasizes a desired function of the first generation of these devices. In terms of the visuomotor adaptation component, further investigation may provide insight into how the brain adapts to a tool such as a neuromotor prosthesis (Lebedev et al. 2005), and, hence, potentially advance the understanding of how to achieve efficient co-adaptation of the brain and decoding model. On a final comparative note, we ran each iteration of our decoding model with a relatively small set of training data composed of 16 (post-exposure) to 32 (pre-, early-, and late-exposure) trials. This small amount of training data is meaningful because it may translate to a substantial reduction in the time required for a patient to gain mastery over the control of a neuromotor prosthesis.

What remains to be elucidated is whether the decoding method presented in this report will also be applicable to EEG, which is better suited than MEG for an ambulatory prosthetic system. In terms of EEG-based decoding of movement parameters, several recent studies have decoded the direction of hand movement (Hammon et al. 2008; Waldert et al. 2008), but, to our knowledge, researchers have yet to report successful decoding of continuous hand position or velocity from EEG (a comprehensive search in peer-reviewed journals did not produce any studies). In the future, we will apply our decoding method to EEG signals to examine the application of this noninvasive modality to continuous, complex control of a neuromotor prosthesis.

Chapter 2: Reconstructing three-dimensional hand movements from noninvasive electroencephalographic signals

The material contained in this chapter is published as Bradberry TJ, Gentili RJ, Contreras-Vidal JL (2010) Reconstructing three-dimensional hand movements from noninvasive electroencephalographic signals. J Neurosci 30:3432–3437. Supplemental material in the journal publication has been incorporated into the main text of this dissertation chapter.

Abstract

It is generally thought that the signal-to-noise ratio, the bandwidth, and the information content of neural data acquired via noninvasive scalp electroencephalography (EEG) are insufficient to extract detailed information about natural, multijoint movements of the upper limb. Here, we challenge this assumption by continuously decoding three-dimensional (3D) hand velocity from neural data acquired from the scalp with 55-channel EEG during a 3D center-out reaching task. To preserve ecological validity, five subjects self-initiated reaches and self-selected targets. Eye movements were controlled so they would not confound the interpretation of the results. With only 34 sensors, the correlation between measured and reconstructed velocity profiles compared reasonably well to that reported by studies that decoded hand kinematics from neural activity acquired intracranially. We subsequently examined the individual contributions of EEG sensors to decoding to find substantial involvement of scalp areas over the sensorimotor cortex

contralateral to the reaching hand. Using standardized low-resolution brain electromagnetic tomography (sLORETA), we identified distributed current density sources related to hand velocity in the contralateral precentral gyrus, postcentral gyrus, and inferior parietal lobule. Furthermore, we discovered that movement variability negatively correlated with decoding accuracy, a finding to consider during the development of brain–computer interface systems. Overall, the ability to continuously decode 3D hand velocity from EEG during natural, center-out reaching holds promise for the furtherance of noninvasive neuromotor prostheses for movement-impaired individuals.

Introduction

In the last decade, research into the neural coding of movement has generated enthusiasm for its potential to restore function to movement-impaired individuals. The field of brain–computer interface (BCI) systems deals with interpreting the neural code and generating commands to control an assistive device. To this end, researchers have extracted hand trajectories or velocity profiles from neuronal signals acquired with electrodes seated directly into cortical tissue and, in some cases, used these kinematics to command a robotic arm in real time (Wessberg et al. 2000; Serruya et al. 2002; Taylor et al. 2002; Hochberg et al. 2006; Kim et al. 2006; Mulliken et al. 2008; Truccolo et al. 2008; Velliste et al. 2008). Investigators have also extracted hand kinematics from intracranial local field potentials obtained through less invasive electrocorticography (Schalk et al. 2007; Pistohl et al. 2008; Sanchez et al. 2008).

In contrast to decoding studies that acquired intracranial neural activity, little work has been done to continuously decode natural, multijoint hand kinematics from neural signals acquired noninvasively. Only a few studies report continuous decoding of two-dimensional (2D) hand and tool kinematics from magnetoencephalography (MEG) (Georgopoulos et al. 2005; Jerbi et al. 2007; Bradberry et al. 2008, 2009a). Although MEG demonstrates a proof of concept, it is immobile and therefore unsuitable for practical BCI systems. However, electroencephalography (EEG) is suitable for practical BCI systems, but, with the exception of our preliminary study (Bradberry et al. 2009b), researchers have not demonstrated continuous decoding of hand kinematics from EEG. Instead, most EEG studies have discretely classified the direction/speed of 2D hand/wrist movements or different motor imagery tasks on a single-trial basis (Mellinger et al. 2007; Hammon et al. 2008; Waldert et al. 2008; Gu et al. 2009), or they have demonstrated 2D continuous control of a cursor through biofeedback training (Wolpaw and McFarland 2004). The lack of attention to reconstructing kinematics of natural hand movements from EEG could be because some researchers consider training subjects to modulate EEG activity, independent of reconstructing hand kinematics, to suffice for 2D control (Wolpaw and McFarland 2004). The lack of attention could also be due to the assumption that EEG signals lack sufficient signal-to-noise ratio, bandwidth, and information content to decode hand kinematics (Lebedev and Nicolelis 2006).

To examine our hypothesis that kinematics of natural hand movements are decodable from EEG signals and, hence, may serve as new signals for controlling neuromotor prostheses, we aimed to continuously extract hand velocity from signals collected during

a three-dimensional (3D) center-out reaching task. To assure a realistic task, subjects were not cued: they chose which target to acquire and when to initiate movement. Since EEG coupled with our decoding method facilitated the investigation of sensor contributions to decoding with high temporal resolution, we examined the location of salient sensors across time lags. Using standardized low-resolution brain electromagnetic tomography (sLORETA) (Pascual-Marqui 2002), we further estimated the sources most involved in encoding hand velocity. Moreover, we investigated the relationship between decoding accuracy and movement variability.

Materials and methods

Experimental procedure

The Institutional Review Board of the University of Maryland at College Park approved the experimental procedure. After giving informed consent, five healthy, right-handed subjects sat upright in a chair and executed self-initiated center-out reaches to self-selected push button targets near eye-level (Fig. 2.1). We instructed subjects to attempt to make uniformly distributed random selections of the eight targets without counting. The elbow of the reaching arm was unsupported, and the non-reaching arm relaxed in the lap. Subjects took approximately 4 s to reach to the peripheral target and then return to the center target. To mitigate the influence of eye movements on reconstruction, subjects were instructed to fixate an LED on the center target throughout data collection and to only blink when their hand was resting at the center target. To ensure the minimization of eye movements, a researcher monitored the subjects' eyes during data collection, and the correlation between electro-ocular activity and hand kinematics was analyzed off-line

(see section on eye movement analysis). For each subject, the experiment concluded after each target was acquired at least ten times. While the required movements were familiar to the subjects, none of the subjects had previous experience with the task.

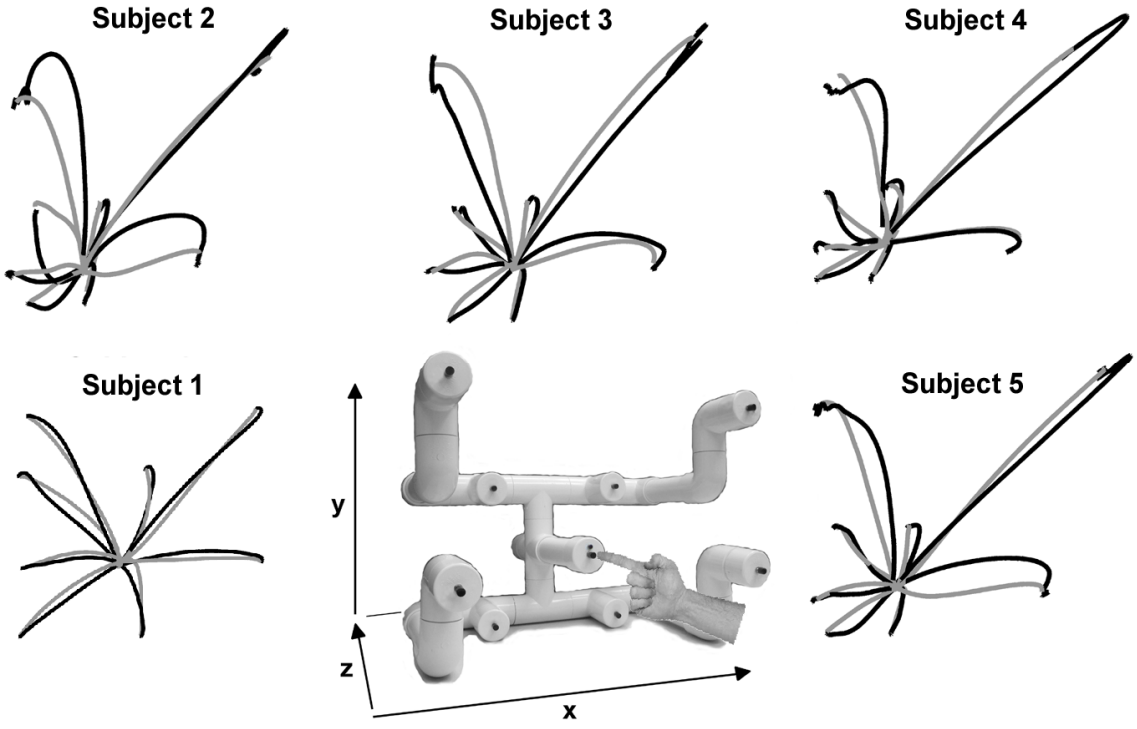

Fig. 2.1. Experimental setup and finger paths. The reaching apparatus is shown in the middle along with the Cartesian coordinate system we employed. The distance from the center position to each of the targets was approximately 22 cm. Mean finger paths for center-to-target (black) and target-to-center (gray) movements exhibited movement variability among subjects.

Data collection

A 64-sensor Electro-Cap was placed on the head according to the extended International 10-20 system with ear-linked reference and used to collect 58 channels of EEG activity. Continuous EEG signals were sampled at 1000 Hz and amplified 500 times via a Synamps I acquisition system and Neuroscan v.4.2 software. Additionally the EEG signals were band-pass filtered from 0.5 to 100 Hz and notch filtered at 60 Hz. Electro-ocular activity was measured with a bipolar sensor montage with sensors attached superior and inferior to the orbital fossa of the right eye for vertical eye movements and to the external canthi for horizontal eye movements. Hand position was sampled at 100 Hz using an Optotrak motion sensing system (Northern Digital, Inc) that tracked an infrared LED secured to the fingertip with double-sided adhesive tape. Event markers of push button presses and releases were sent from the apparatus containing the push buttons to the Neuroscan and Optotrak systems for off-line synchronization of EEG and kinematic data.

Signal pre-processing

For computational efficiency and to match the sampling rate of the kinematic data, the EEG data were decimated from 1 kHz to 100 Hz by applying a low-pass anti-aliasing filter with a cutoff frequency of 40 Hz and then downsampling by a factor of 10. A zero-phase, fourth-order, low-pass Butterworth filter with a cutoff frequency of 1 Hz was then applied to the kinematic and EEG data. The cutoff frequency was determined experimentally with influence by previous noninvasive and ECoG studies that demonstrated the importance of low frequencies for noninvasive decoding (Jerbi et al.

2007; Schalk et al. 2007; Waldert et al. 2008; Bradberry et al. 2008, 2009a). Next, the temporal difference of the EEG data was computed (i.e., $v_n[t] = \tilde{v}_n[t] - \tilde{v}_n[t-1]$ where $v_n[t]$ and $\tilde{v}_n[t]$ are respectively the backward-differenced and pre-differenced EEG voltage of sensor n at time t). In order to examine relative sensor contributions in the scalp map analysis described in a section below, data from each EEG sensor were standardized according to Eq. (2.1):

$$S_n[t] = \frac{v_n[t] - \mu_{v_n}}{\sigma_{v_n}} \quad \text{for all } n \text{ from 1 to } N \tag{2.1}$$

where $S_n[t]$ and $v_n[t]$ are respectively the standardized and differenced voltage at sensor n at time t, μ_{v_n} and σ_{v_n} are the mean and standard deviation of v_n respectively, and N is the number of sensors.

Decoding method

To continuously decode hand velocity from the EEG signals, a linear decoding model was employed similar to that described by Georgopoulos et al. (2005) for MEG signals. In general, the model finds a linear combination of past and present time series data from multiple EEG sensors that reconstructs the current kinematic sample of a dimension of hand velocity. In equation form:

$$x[t] - x[t-1] = a_x + \sum_{n=1}^{N}\sum_{k=0}^{L} b_{nkx} S_n[t-k] \tag{2.2}$$

$$y[t] - y[t-1] = a_y + \sum_{n=1}^{N}\sum_{k=0}^{L} b_{nky} S_n[t-k] \tag{2.3}$$

$$z[t] - z[t-1] = a_z + \sum_{n=1}^{N}\sum_{k=0}^{L} b_{nkz} S_n[t-k] \quad (2.4)$$

where $x[t]-x[t-1]$, $y[t]-y[t-1]$, and $z[t]-z[t-1]$ are the horizontal, vertical, and depth velocities of the hand at time sample *t* respectively, *N* is the number of EEG sensors, *L* (= 10) is the number of time lags, $S_n[t-k]$ is the standardized difference in voltage measured at EEG sensor *n* at time lag *k*, and the *a* and *b* variables are weights obtained through multiple linear regression. The number of lags (*L*=10, corresponding to 100 ms) was chosen based on a previous study that reconstructed hand kinematics from neural signals acquired with MEG (Bradberry et al. 2009a). The three most frontal sensors (FP1, FPZ, and FP2 of the International 10-20 system) were excluded from the analysis to further mitigate the influence of any eye movements on reconstruction, resulting in an *N* of 55 sensors.

For each subject, the collected continuous data contained approximately 80 trials. An 8x8-fold cross-validation procedure was employed to assess the decoding accuracy. In this procedure, the entire continuous data were divided into 8 parts, 7 parts were used for training, and the remaining part was used for testing. The velocity data and EEG data were synchronized, so that if *m* samples of velocity were to be reconstructed then the aligned *m* samples of EEG data from a single sensor were used along with 10 lagged versions of these *m* EEG samples for a total of *m*(10 + 1) samples per sensor (plus one for the offset *a*). Based on the sampling rate of 100 Hz and collection duration of approximately 5 minutes per subject, *m* was about 3750 samples per training fold and 26,250 samples per testing fold. The cross-validation procedure was considered complete

when each of the 8 combinations of training and testing data were exhausted, and the mean Pearson correlation coefficient (*r*) between measured and reconstructed kinematics was computed across folds. Prior to computing *r*, the kinematic signals were smoothed with a zero-phase, fourth-order, low-pass Butterworth filter with a cutoff frequency of 1 Hz.

Sensor sensitivity curves

Curves depicting the relationship between decoding accuracy and the number of sensors used in the decoding method were plotted for the *x*, *y*, and *z* dimensions of hand velocity. First, for each subject, each of the 55 sensors was assigned a rank according to

$$R_n = \frac{1}{L+1}\sum_{k=0}^{L}\sqrt{b_{nkx}{}^2 + b_{nky}{}^2 + b_{nkz}{}^2} \qquad \text{for all } n \text{ from 1 to } N \tag{2.5}$$

where R_n is the rank of sensor *n*, and the *b* variables are the best regression weights. This ranking procedure is similar to the one described by Sanchez et al. (2004). Next, the decoding method with cross-validation as described above and ranking method were iteratively executed using backward elimination with a decrement step of three (52 highest-ranked sensors, 49 highest-ranked sensors, 46 highest-ranked sensors, etc.). The mean and standard error of the mean (SEM) of *r* values computed across subjects were plotted against the number of sensors.

Scalp maps of sensor contributions

To graphically assess the relative contributions of scalp regions to the reconstruction of hand velocity, the across-subject mean of the magnitude of the best *b* vectors (from Eqs.

(2.2) – (2.4)) was projected onto a time series (-100–0 ms in increments of 10 ms) of scalp maps. These spatial renderings of sensor contributions were produced by the topoplot function of EEGLAB, an open-source MATLAB toolbox for electrophysiological data processing (Delorme and Makeig 2004; http://sccn.ucsd.edu/eeglab/), that performs biharmonic spline interpolation of the sensor values before plotting them (Sandwell 1987). To examine which time lags were the most important for decoding, for each scalp map, the percentage of

reconstruction contribution was defined as

$$\%T_i = 100\% \times \frac{\sum_{n=1}^{N} \sqrt{{b_{nix}}^2 + {b_{niy}}^2 + {b_{niz}}^2}}{\sum_{n=1}^{N} \sum_{k=0}^{L} \sqrt{{b_{nkx}}^2 + {b_{nky}}^2 + {b_{nkz}}^2}} \quad \text{for all } i \text{ from 0 to } L \tag{2.6}$$

where $\%T_i$ is the percentage of reconstruction contribution for a scalp map at time lag i.

Source estimation with sLORETA

To better estimate the sources of hand velocity encoding, we used standardized low-resolution brain electromagnetic tomography (sLORETA) software version 20081104 (Pascual-Marqui 2002; http://www.uzh.ch/keyinst/loreta.htm). Preprocessed EEG signals from all 55 channels for each subject were fed to sLORETA to estimate current sources. These EEG signals had been pre-processed in the same manner as for decoding: standardized, downsampled, and low-pass filtered. First, r values were computed between the squared time series of each of the 55 sensors with the 6239 time series from the sLORETA solution and then averaged across subjects. Second, the maximum r was assigned to each voxel after being multiplied by the regression weight b (from Eqs. (2.2)

–(2.4)) of its associated sensor. The regression weights had been pulled from the regression solution at time lag −60 ms, which had the highest percentage of reconstruction contribution. Third, for visualization purposes, the highest 5% of the voxels (*r* values weighted by *b*) were set to the value one, and the rest of the *r* values were set to zero. Finally these binary-thresholded *r* values were plotted onto axial slices of the brain from the Colin27 volume (Holmes et al. 1998), the magnetic resonance imaging (MRI) template that best illustrated our regions of interest. All reported coordinates of regions of interest are in Montreal Neurological Institute (MNI) space.

Movement variability

For each subject, three measures of movement variability were computed: the coefficient of variation (CV) for movement time (MT), the CV for movement length (ML), and the kurtosis of movement. MT and ML were computed on a trial basis with a trial defined as the release of a pushbutton to the press of a pushbutton (center-to-target or target-to-center). The mean and SD of the measures were then computed, and the SD was divided by the mean to produce the CV. Kurtosis was defined as

$$k = \frac{E(h - \mu_h)^4}{\sigma_h{}^4} - 3 \tag{2.7}$$

where *k* is the kurtosis, *E*() is the expected value operator, *h* is the hand velocity, and μ_h and σ_h are respectively the mean and SD of the hand velocity. Single trials of velocity profiles for *x*, *y*, and *z* dimensions were resampled to normalize for length and then concatenated before computing kurtosis. The relationship between movement variability and decoding accuracy was examined by computing *r* between the quantities. The sample

sizes were small (n = 5) for decoding accuracy and each measure of movement variability, so 10,000 r values were bootstrapped for each comparison, and the median and confidence intervals of the resultant non-Gaussian distributions were calculated using the bias-corrected and accelerated (BC_a) percentile method (Efron and Tibshirani 1998).

Eye movement analysis

When reconstructing a behavioral variable from neural activity, it is important to ensure the minimization of co-occurring, correlated behavioral variables that may simultaneously influence neural activity. To this end for our reaching task, in addition to instructing subjects to fixate a center LED, we needed to confirm that electrooculographic (EOG) activity only minimally correlated with hand velocity. We computed r values between EOG velocity and hand velocity across 10 time lags (-100 ms) with both signals low-pass filtered at 1 Hz as in the case of hand kinematic decoding from EEG.

Results

Our EEG decoding method reconstructed 3D hand-velocity profiles reasonably well. We quantified the decoding accuracy by computing the mean of Pearson's r between measured and reconstructed hand velocity across cross-validation folds. For y and z velocities, the decoding accuracy peaked at 0.38 and 0.32, respectively, with only 34 sensors (Fig. 2.2A,B). For x velocity with 34 sensors, the decoding accuracy of 0.19 remained relatively unaffected by the number of sensors. Thus, we used 34 sensors for subsequent analyses. In addition to quantitatively analyzing decoding accuracy, visually

comparing reconstructed and measured velocity profiles confirmed their similarities (Fig. 2.2C).

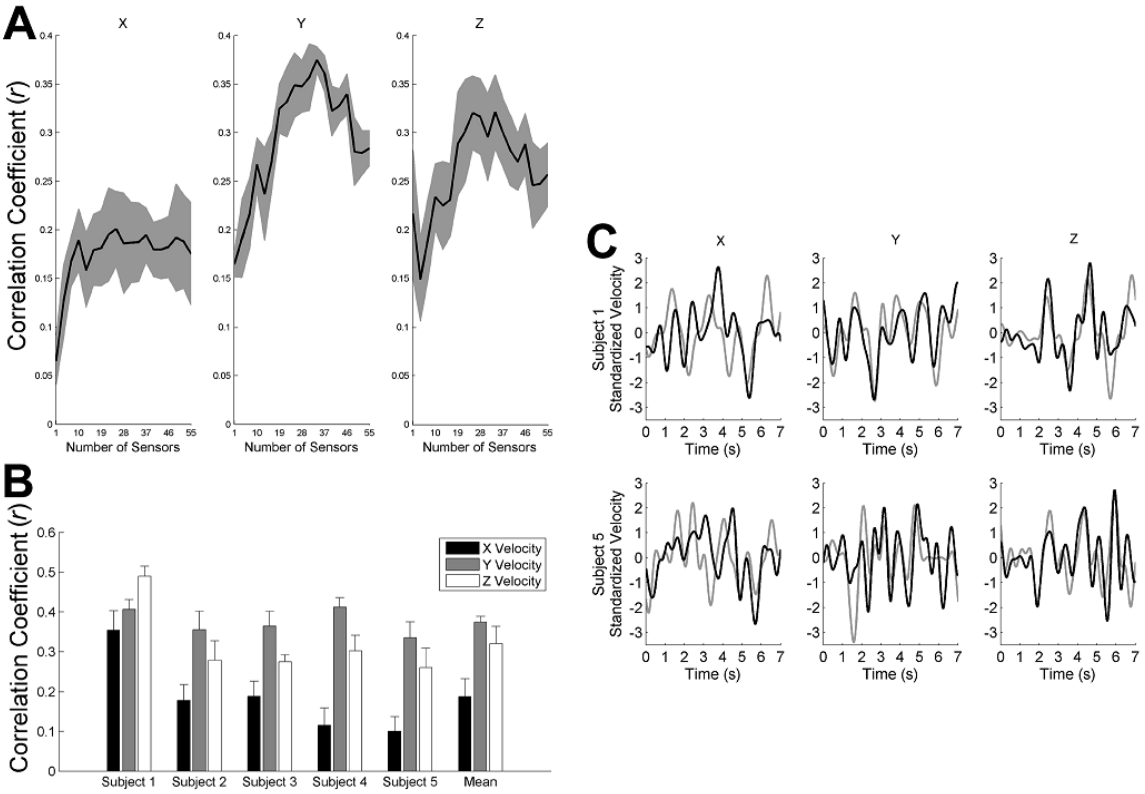

Fig. 2.2. EEG decoding accuracy of hand velocity. (A) The mean (black) ± SEM (gray) of the *r* values across subjects (n = 5) vs. the number of sensors exhibited a peak at 34 sensors. (B) With 34 sensors, we computed the mean ± SEM of the *r* values across cross-validation folds (n = 8) for each subject for *x* (black), *y* (gray), and *z* (white) velocities. (C) Reconstructed (black) and measured (gray) velocity profiles demonstrated similarities. Exemplar velocity profiles from the subjects with the best (Subject 1, top row) and worst (Subject 5, bottom row) decoding accuracies are shown.

Scalp maps depicted the contributions of the 34 sensors as a network of frontal, central, and parietal regions (Fig. 2.3A). Within this network, sensor CP3 made the greatest contribution. Interestingly, CP3 lies roughly above the primary sensorimotor cortex that is contralateral to the reaching hand. Concerning time lags, EEG data from 60 ms in the past supplied the most information with 16.0% of the total contribution. At 60 ms, we localized the EEG sources to confirm that the primary sensorimotor cortex (precentral gyrus and postcentral gyrus) was indeed a major contributor along with the inferior parietal lobule (IPL) (Fig. 2.3B).

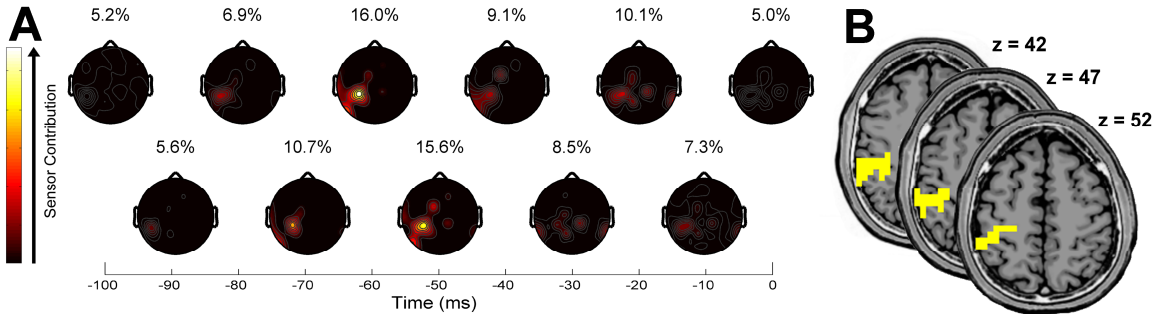

Fig. 2.3. Scalp and current sources that encoded hand velocity. (A) Mean (n = 5) scalp maps of the best 34 sensors revealed a network of frontal, central, and parietal involvement along with a large individual contribution from sensor CP3. Light and dark colors represent high and low contributors, respectively. Each scalp map with its percentage contribution is displayed above its associated 10 ms time lag, revealing the 16.0% maximal contribution of EEG data at 60 ms in the past. (B) We overlaid localized sources (yellow) from 60 ms in the past onto MRI structural images to reveal the involvement of the precentral gyrus (x = –30, y = –30, z = 52), postcentral gyrus (x = –35, y = –30, z = 47), and IPL (x = –35, y = –36, z = 42).

Additionally, we compared the relationship between decoding accuracy, shown in Fig. 2.2B, and movement variability. To quantify movement variability, we computed the CV for MT and ML (Fig. 2.4A) and the kurtosis of the velocity profiles (Fig. 2.4B). The high kurtosis values indicated outlier-prone, super-Gaussian distributions (kurtosis, >0). We found that movement variability negatively correlated with decoding accuracy (Fig. 2.4C). Fig. 2.1 aids in visually depicting this relationship by showing that subject 1, with the best decoding accuracy, performed straighter reaches.

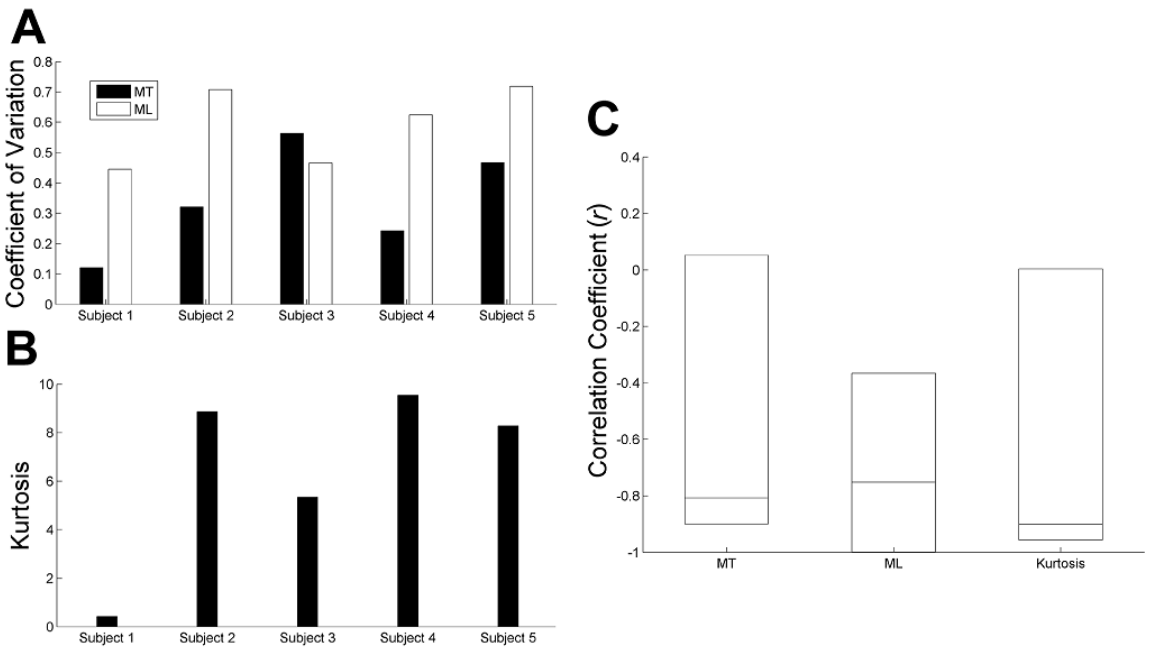

Fig. 2.4. Relationship between movement variability and decoding accuracy. (A) The CVs for MT (black) and ML (white) ranged across subjects. (B) The kurtosis of the velocity profiles also varied across subjects. (C) All movement variability measures demonstrated high negative correlations with the decoding accuracy shown in Fig. 2.2B. Rectangles demarcate the confidence intervals for the bootstrapped *r* values, with each

rectangle possessing a horizontal line at the median. The confidence intervals are 70, 90, and 70%, respectively, for MT, ML, and kurtosis.

We computed *r* values between EOG velocity and hand velocity across time lags to confirm that they only minimally correlated (Fig. 2.5).

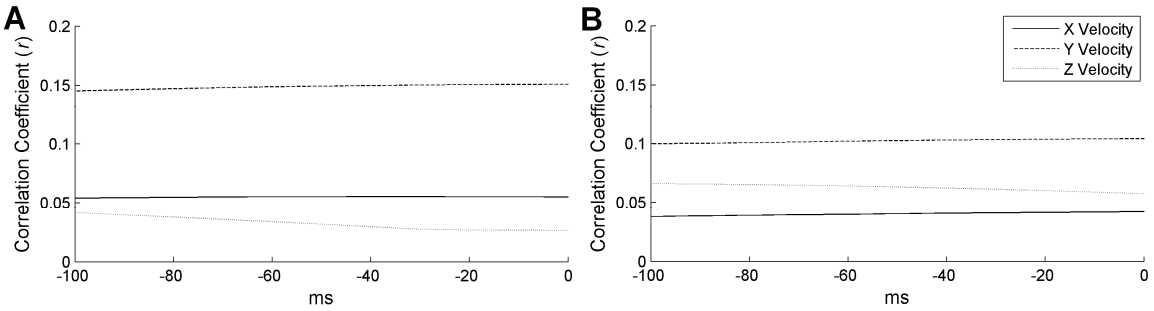

Fig. 2.5. Cross-correlation between EOG velocity and hand velocity. We computed *r* values between EOG velocity and hand velocity across 10 time lags (-100 ms) with both signals low-pass filtered at 1 Hz. The across-subject mean (n = 5) *r* values exhibited low correlation of vertical (A) and horizontal (B) EOG velocities with *x* (solid), *y* (dashed), and *z* (dotted) dimensions of hand velocity.

Discussion

In the last decade, researchers have pushed the boundaries of noninvasive neural decoding in the interest of developing BCI systems for the movement impaired. To further stretch the limits, we continuously reconstructed 3D hand velocity of natural, multijoint, center-out movements from only 34 channels of EEG data. A sensorimotor network composed of frontal, central, and parietal scalp regions encoded for hand

velocity, with the strongest contributions coming from cortical regions of the precentral gyrus, postcentral gyrus, and IPL at 60 ms in the past. Furthermore, the intersubject variability in movement may explain the intersubject variability in decoding accuracy due to their negative correlation.

The sensor sensitivity curves for *y* and *z* velocities peak at ≈0.35 for 34 sensors before they begin decreasing. A common occurrence in machine learning is that, as the number of input features increases, prediction increases up to a point, then prediction may decrease due to overfitting the model to the training data, which is likely the case here (Alpaydin 2004). The curve for *x* velocity remains nearly flat ≈0.20 after an initial rapid increase (Fig. 2.2A). We made the common assumption that the brain employs a hand-centered Cartesian coordinate system. However, the possibility exists that the brain could represent a different coordinate system (e.g., joint space or multiple interacting frames of reference) or desired muscular activity (Gourtzelidis et al. 2001; Wu and Hatsopoulos 2006, 2007). The dimensions of an alternate representation could correlate better with *y* and *z* velocities than *x* velocity, potentially explaining the uniqueness of the sensitivity curve for *x* velocity. Nonetheless, in future studies when subjects are asked to use motor imagery to control a cursor or virtual arm in 3D via our decoder, we expect their neural activity to adapt to overcome an initial imperfect choice of representation framework, as Ganguly and Carmena (2009) observed in an invasive BCI experiment.

To our knowledge, apart from our preliminary study (Bradberry et al. 2009b), studies on continuously decoding hand kinematics from EEG do not exist. Therefore, we cannot

directly compare our results to the literature. However, two studies report off-line, continuous reconstruction of 3D hand kinematics from intracranial neuronal activity (Wessberg et al. 2000; Kim et al. 2006), and several studies report off-line, continuous reconstruction of 2D hand and tool kinematics from MEG (Georgopoulos et al. 2005; Jerbi et al. 2007; Bradberry et al. 2008, 2009a). Of the MEG investigations, Bradberry et al. (2008, 2009a) exclusively employs a center-out movement paradigm, the *de facto* standard for comparison among decoding studies with BCI implications. These other studies report slightly higher *r* values (Table 2.1), but uniquely our study involves more ambitious experimental settings, such as more reaching targets, greater extent of multijoint movements, self-initiated movements, and self-selected targets.

Strengthening the validity of our decoding results, scalp maps and estimated current sources indicate involvement of the contralateral primary sensorimotor region and the IPL. Other studies confirm that the primary sensorimotor cortex encodes hand kinematics at a microscale (Georgopoulos et al. 1986; Moran and Schwartz 1999; Wessberg et al. 2000; Serruya et al. 2002; Schwartz et al. 2004; Kim et al. 2006), mesoscale (Schalk et al. 2007; Pistohl et al. 2008; Sanchez et al. 2008), and macroscale (Kelso et al. 1998; Jerbi et al. 2007). Several MEG studies report that the IPL also encodes hand kinematics (Jerbi et al. 2007; Bradberry et al. 2009a). Regardless of scale, decoding methods like the one we report here rely on a subsecond history of neural data to reconstruct hand kinematics (Serruya et al. 2002, Sanchez et al. 2008; Bradberry et al. 2009a). Our choice of a 100 ms lag aligns with this convention as well as the rationale that these lags consist of planning activity of the brain associated with the current kinematic sample of the hand.

Furthermore, across lags the sensor contributions initially increase, peak at 60 ms, and then decrease, possibly revealing a temporal tuning curve for our task. Since only low-frequency components of the EEG signals seem to carry information about hand velocity, slow cortical potentials emerge as the best candidates for a neurophysiological interpretation of these findings (Birbaumer et al. 1990).

Table 2.1. Comparison to most relevant off-line decoding studies of hand kinematics

	Subjects	Neural Data	Reaching / Drawing Task	Cued?	r_x	r_y	r_z	average r
Wessberg et al. 2000	monkeys (n = 2)	single units	3D; table→1 of 4 food tray positions→mouth	Yes	0.50*	0.45*	0.65*	0.53
Kim et al. 2006	monkey (n = 1)	single units	3D; table→1 of 4 food tray positions→mouth→ table	Yes	–	–	–	0.44†
Bradberry et al. 2009a	humans (n = 5)	MEG	2D; center of DT→1 of 4 peripheral targets of DT→ center of DT	Yes	0.48‡	0.32‡	–	0.40
Present study	humans (n = 5)	EEG	3D; center PB→1 of 8 peripheral PBs→center PB	No	0.19	0.38	0.32	0.29

DT: drawing tablet, PB: push button

* Since Wessberg et al. (2000) provide the evolution of r over time, and the duration of our task is approximately 5 minutes; we used their reported r_x, r_y, and r_z values at 5 minutes into their task.

† For the Kim et al. (2006) study, we computed the average between their reported r during movement and r during rest for their best decoding method.

‡ For the Bradberry et al. (2009a) study, r_x and r_y were taken from only the pre-exposure phase (no novel visuomotor transformation imposed).

An important topic in BCI research involves how decoding methods may adapt or facilitate user adaptation to novel environments or cognitive states. To evaluate adaptation, the user of a BCI system must receive feedback (e.g., visual or kinesthetic) of imagined movements while manipulating a brain-controlled device in real time. In the future, it will be essential to provide subjects with real-time feedback to investigate their ability to adapt their EEG activity to a fixed decoder (i.e., test the ability of our decoder to generalize). To improve performance, it is expected that subjects will "modify" regression weights by modulating their EEG activity. Decoder generalization has recently been demonstrated and analyzed in monkeys by Ganguly and Carmena (2009). Regarding humans, researchers have not thoroughly analyzed generalization; regardless, comparably impressive 2D control has been demonstrated by sensorimotor rhythms derived from EEG (Wolpaw and McFarland 2004) and single neurons (Hochberg et al. 2006). Given this evidence, we expect our decoding method for EEG to permit 3D brain control by humans in real time.

Regarding the negative correlation between movement variability and decoding accuracy, we offer two potential explanations. For the more technical explanation, increased movement variability could degrade decoding accuracy due to less similar pairs of EEG–kinematic exemplars. Conversely, less movement variability results in more similar exemplars for training. A more neural related explanation is that subjects differ in their ability to perform the task without practice; hence, the strengths of a priori neural representations of the required movements differ. These differing strengths could directly relate to the accuracy with which the representations can be extracted. Indeed, a previous

study confirms that motor learning produces more accurate predictions of movement direction from an ensemble of neuronal activity in primary motor cortex (Cohen and Nicolelis 2004). This finding is important to consider as real-time BCI systems based on our decoder are investigated in the future.

In conclusion, despite the common assumption that EEG signals do not possess decodable information about detailed, complex hand movements, we demonstrate otherwise. The locations of the most important sensors to decoding are interpretable in light of previous studies and corroborate our claims. In the near future, the question should be addressed of how well subjects can adapt to our decoder of 3D kinematics when feedback of the decoder output is provided.

Funding

This work was financially supported by La Fondation Motrice (Paris, France) (R.J.G.).

Chapter 3: A noninvasive brain-computer interface system with efficient decoder calibration based on observation of cursor movement

Abstract

Most current noninvasive brain-computer interface (BCI) systems aimed at cursor control are based on neural signals acquired with electroencephalography (EEG). A limitation of these current BCI systems is the lengthy training time (weeks to months) required by users to achieve satisfactory multidimensional control. To address this limitation, we investigated a novel approach for continuously decoding imagined movements from EEG signals in a BCI experiment involving five subjects that performed a three-phase task: calibration, practice, and target acquisition. During the calibration phase, subjects imagined moving their right arm/finger to track a cursor that moved in two dimensions on a computer screen (10 min). A decoding initialization procedure was then executed to find the decoder parameters that best mapped 34 EEG signals to observed horizontal and vertical cursor velocities (~10 min) (Bradberry et al. 2010 *J Neurosci* 30). Through subsequent investigation of the cortical sources that encoded for observed cursor velocity, a large neural network that comprised brain regions considered a part of the human mirror neuron system (MNS) was engaged. During the practice phase, after an initial manual adjustment of cursor speed to comfortable values by investigators (~10 min), subjects used the calibrated decoder to move the cursor with their thoughts in two dimensions as desired without task constraints for 10 min. During the target acquisition

phase, subjects used their thoughts to move the cursor to a target that appeared pseudorandomly at the top, bottom, left, or right side of the computer screen. If subjects did not acquire the target within 15s, the trial was aborted, and a new target appeared. Four 10-minute runs of target acquisition were performed. The mean ± standard error (SE) of the target hit rate was 73 ± 4% across subjects and runs. A snapshot of cortical sources that maximally encoded for cursor velocity during the target acquisition phase primarily differed from that of the calibration phase by revealing a more widespread involvement of the primary sensorimotor cortex and decreased involvement of the putative MNS. Our results suggest that the reported approach to continuously decoding imagined movements from EEG signals substantially reduces training time for noninvasive BCI systems and allows for unique insights into the cortical regions involved in encoding imagined and observed movements under different task constraints. Moreover, our decoding method serves as a novel tool for studying the development and plasticity of neural representations underlying action observation and action production at the macroscale afforded by EEG.

Introduction

Brain-computer interface (BCI) systems may potentially provide movement-impaired persons with the ability to interact with their environment using only their thoughts to control assistive devices such as communication programs and smart artificial arms. Currently the most promising BCI systems rely on neural signals acquired noninvasively with electroencephalography (EEG) (Wolpaw and McFarland 2004) or invasively with

microelectrode arrays seated into cortical tissue (Hochberg et al. 2006) or electrocorticography (ECoG) (Schalk et al. 2008).

Noninvasive EEG-based BCI systems for 2D cursor control require subjects to learn to modulate sensorimotor rhythms to move a cursor to acquire targets (Wolpaw and McFarland 2004). These types of studies based on sensorimotor rhythms required weeks to months of training before satisfactory levels of performance are attained. Relative to EEG signals, the increased signal-to-noise ratio and bandwidth of invasively acquired neural data are commonly thought to be factors that reduce the training time required by users of invasive BCI systems (Schalk et al. 2008). In addition, studies of tetraplegic humans with implanted microelectrode arrays have exclusively demonstrated 2D control of a cursor through imagined natural movement (Hochberg et al. 2006; Kim et al. 2008). This decoding of imagined *natural movement* is also a likely factor in reduced training time.

However, recently several off-line decoding studies demonstrated the reconstruction of cursor and hand kinematics from noninvasive magnetoencephalography (MEG) and EEG (Bradberry et al. 2009a, 2010). The noise and bandwidth limitations of the noninvasively acquired signals did not impede decoding kinematics of *natural movement*. This finding infers that a BCI system based on the decoding method reported in those studies may require little training time. In this study, we sought to investigate the use of the decoding method reported in those studies in an EEG-based BCI system during a single session lasting less than two hours that required only a brief (10 min) calibration phase.

Moreover, we hypothesized that if the neural representation of visual movement during observation could be decoded, this information could be harnessed for brain-control of a computer cursor as previously demonstrated by invasive studies (Hochberg et al. 2006; Kim et al. 2008). Thus, we examined the involvement of neural regions in encoding cursor velocity during observation of computer-controlled cursor movement and during tasks requiring a brain-controlled cursor to acquire targets in 2D space.

Materials and methods

Experimental tasks

The Institutional Review Board of the University of Maryland at College Park approved the experimental procedure. After giving informed consent, five healthy, right-handed subjects performed a three-phase task: calibration, practice, and target acquisition. In all phases, their EEG signals were acquired while they sat upright in a chair with hands resting in their laps at arm's length away from a computer monitor that displayed a workspace of dimensions 30 x 30 cm and a cursor of diameter 1.5 cm (0.20% of workspace) (Fig. 3.1). Subjects were instructed to remain still and relax their muscles to reduce the introduction of artifacts into the EEG recordings.

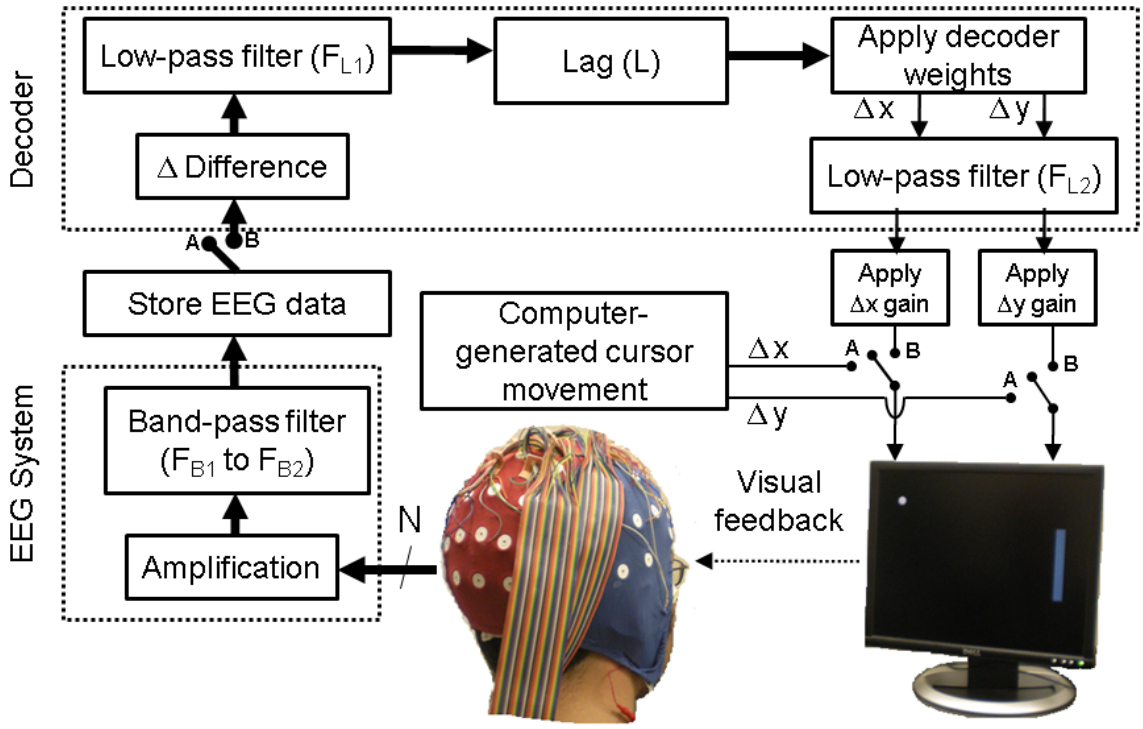

Fig. 3.1. Diagram of data processing flow for EEG-based BCI experiment. When the switches are in position A, the system is in observation/calibration mode. In observation/calibration mode, a subject observes a replay of a pilot subject's cursor movements on a computer screen while data from N (34) EEG sensors are continuously acquired by an EEG system that amplifies and band-pass filters the data from F_{B1} (0.01) to F_{B2} (30) Hz before storing them. Afterwards, the EEG data and observed cursor velocity are used to compute the decoder weights. When the switches are in position B, the system is in practice or target acquisition mode. In practice mode, after the EEG data are stored, they are continuously temporally differenced, low-pass filtered at F_{L1} (1) Hz, lagged L (11) times (a lag of 0 also occurs), decoded for cursor velocity by the calibrated decoder from the preceding calibration phase, low-pass filtered again at F_{L2} (1) Hz, and gain adjusted before being displayed on the computer monitor as visual feedback to the

subject. The practice mode differs from the target acquisition mode in that, during practice, the gains preceding the cursor display are manually adjusted by investigators (difference not depicted in diagram), and no targets are present on the screen (unlike the screen in the diagram that shows a target on the right). In target acquisition mode, subjects attempt to move the cursor to targets that appear pseudorandomly at the left, right, top, or bottom of the screen.

Calibration

During the 10-minute calibration phase, subjects were instructed to imagine moving their right arm/finger to track a computer-controlled cursor that moved in two dimensions on the computer screen. The movements of the computer-controlled cursor were generated by replaying a pilot subject's brain-controlled cursor movements from one of his practice runs (this pilot subject did not participate as one of the five subjects in this study). Histograms of the horizontal and vertical positions and velocities of the computer-controlled movements indicated approximately uniform coverage of the workspace and biological motion respectively (Fig. 3.2). The decoding procedure described in a section below was subsequently executed (~10 min of computation time) to calibrate the decoder so that it best mapped the EEG signals to observed horizontal and vertical cursor velocities. During pilot testing, we discovered that asking subjects to visually fixate the center of the workspace while simultaneously tracking the cursor added attentional demands that burdened the subjects and likely compromised the decoding; therefore, we told subjects they were free to move their eyes but to always maintain eye contact and spatial attention with the moving cursor.

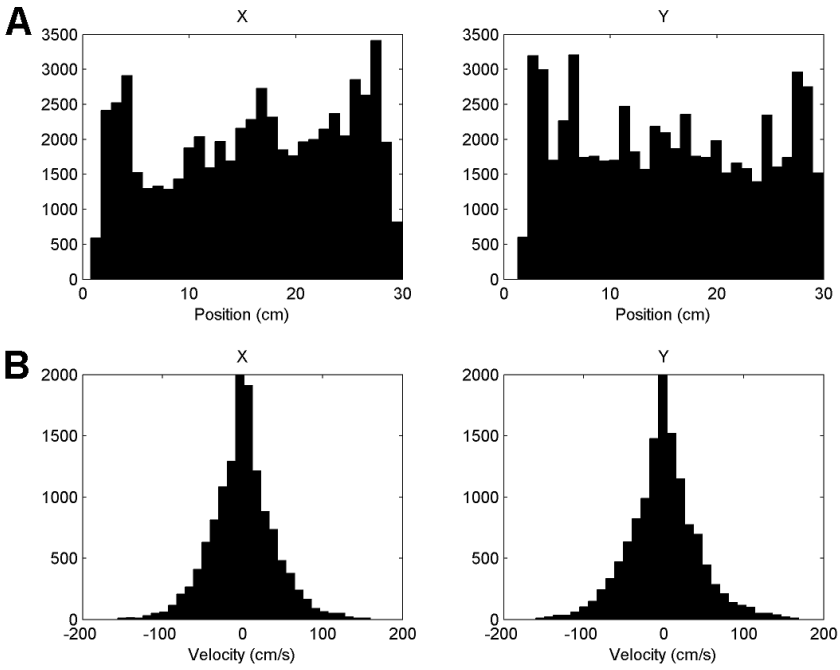

Fig. 3.2. Histograms of observed cursor kinematics during the calibration phase. (A) Histograms of horizontal (left) and vertical (right) positions indicated approximately uniform coverage of the workspace. (B) Histograms of horizontal (left) and vertical (right) positions inferred movements with bell-shaped velocity profiles (although these are more super-Gaussian than typical point-to-point movements), indicative of biological motion. The velocity histograms actual peak near 5000 but were truncated so the shape of the base could be viewed.

Practice

During the practice phase, the subjects used the calibrated decoder to attempt to move the cursor with their thoughts in two dimensions as desired (without task constraints). They were instructed to figure out for themselves how to best control the cursor by exploring the workspace. They were also informed as to where the target locations would be in the

target acquisition phase that would follow. Again, they were free to move their eyes. During the initial portion of the practice phase, horizontal and vertical gains were independently adjusted by the investigators to balance cursor speed so that the velocity of the brain-controlled cursor was comfortable to the subjects. After the gains were manually adjusted (~10 min), subjects practiced moving the cursor without task constraints for 10 minutes.

Target acquisition

During the target acquisition phase, subjects were instructed to use their thoughts to move the cursor in two dimensions to reach a peripheral target (1.3% of workspace) that would appear pseudorandomly at the top, bottom, left, or right side of the computer screen (Fig. 3.1). They were informed that if they did not did not acquire the target within 15 s, a new target would appear, and the trial was considered a failure. Four 10-minute runs of target acquisition were performed with a 1-minute rest interval between runs.

Data acquisition

A 64-sensor Electro-Cap was placed on the head according to the extended International 10-20 system with ear-linked reference and used to collect 58 channels of EEG activity. Continuous EEG signals were sampled at 100 Hz and amplified 1000 times via a Synamps I acquisition system and Neuroscan v4.3 software. Additionally the EEG signals were band-pass filtered from 0.01 to 30 Hz. Electroocular (EOG) activity was measured with a bipolar sensor montage with sensors attached superior and inferior to the orbital fossa of the right eye for vertical eye movements and to the external canthi for

horizontal eye movements. The EEG signals were continuously sent to the BCI2000 software system for online processing and storage (Schalk et al. 2004, http://bci2000.org). BCI2000 was responsible for moving the cursor based on our decoder function, which we integrated into the open source software system. BCI2000 was also responsible for storing cursor movement data as well as collecting markers of workspace events such as target acquisition. Electromyographic (EMG) signals were amplified and collected at 2000 Hz from two bipolar surface electrodes over the flexor carpi radialis and extensor digitorum muscles of the right forearm using an Aurion ZeroWire system (10-1000 Hz bandwidth, constant electrode gain of 1000).

Decoding method

The decoding method employed in this study has been previously described so will only briefly be described here (Bradberry et al. 2010). First, a fourth-order, low-pass Butterworth filter with a cutoff frequency of 1 Hz was applied to the kinematic and EEG data. Next, the first-order temporal difference of the EEG data was computed. To continuously decode cursor velocity from the EEG signals, a linear decoding model was employed:

$$x[t] - x[t-1] = a_x + \sum_{n=1}^{N}\sum_{k=0}^{L} b_{nkx} S_n[t-k] \tag{3.1}$$

$$y[t] - y[t-1] = a_y + \sum_{n=1}^{N}\sum_{k=0}^{L} b_{nky} S_n[t-k] \tag{3.2}$$

where $x[t]-x[t-1]$ and $y[t]-y[t-1]$ are the horizontal and vertical velocities of the cursor at time sample t respectively, N is the number of EEG sensors, L (= 11) is the number of

time lags, $S_n[t-k]$ is the difference in voltage measured at EEG sensor *n* at time lag *k*, and the *a* and *b* variables are weights obtained through multiple linear regression. Only the most important sensors (*N* = 34) for velocity reconstruction found in Bradberry et al. (2010) were used for decoding.

For the calibration phase, a 10x10-fold cross-validation procedure was employed to assess the reconstruction accuracy of observed cursor velocity from EEG signals. In this procedure, the entire continuous data were divided into 10 parts, 9 parts were used for training, and the remaining part was used for testing. The cross-validation procedure was considered complete when each of the 10 combinations of training and testing data were exhausted, and the mean Pearson correlation coefficient (*r*) between measured and reconstructed kinematics was computed across folds. Prior to computing *r*, the kinematic signals were smoothed with a fourth-order, low-pass Butterworth filter with a cutoff frequency of 1 Hz. For the ensuing practice and target acquisition phases, the regression weights (*a* and *b* variables) for the cross-validation fold with the highest *r* were used for online decoding.

Scalp maps of sensor contributions

To graphically assess the relative contributions of scalp regions to the reconstruction of cursor velocity, the decoding procedure described in the section above was run on standardized EEG signals, and the across-subject mean of the magnitude of the best *b* vectors (from Eqs. (3.2) and (3.3)) was projected onto a time series (-110–0 ms in increments of 10 ms) of scalp maps. These spatial renderings of sensor contributions

were produced by the topoplot function of EEGLAB, an open-source MATLAB toolbox for electrophysiological data processing (Delorme and Makeig 2004; http://sccn.ucsd.edu/eeglab/), that performs biharmonic spline interpolation of the sensor values before plotting them (Sandwell 1987). To examine which time lags were the most important for decoding, for each scalp map, the percentage of reconstruction contribution was defined as

$$\%T_i = 100\% \times \frac{\sum_{n=1}^{N} \sqrt{{b_{nix}}^2 + {b_{niy}}^2 + {b_{niz}}^2}}{\sum_{n=1}^{N} \sum_{k=0}^{L} \sqrt{{b_{nkx}}^2 + {b_{nky}}^2 + {b_{nkz}}^2}} \tag{3.3}$$

for all i from 0 to L, where $\%T_i$ is the percentage of reconstruction contribution for a scalp map at time lag i.

Source estimation with sLORETA

To better estimate the sources of cursor velocity encoding, we used standardized low-resolution brain electromagnetic tomography (sLORETA) software version 20081104 (Pascual-Marqui 2002; http://www.uzh.ch/keyinst/loreta.htm). Preprocessed (low-pass filtered and differenced) EEG signals from all 34 channels for each subject were fed to sLORETA to estimate current sources. First, r values were computed between the squared time series of each of the 34 sensors with the 6239 time series from the sLORETA solution and then averaged across subjects. Second, the mean of the r values multiplied by the regression weights b (from Eqs. (3.1) and (3.2)) of their associated sensors were assigned to each voxel. The regression weights had been pulled from the regression solution at the time lag with maximum $\%T_i$, which had the highest percentage

of reconstruction contribution. Third, for visualization purposes, the upper quartile of voxels (*r* values weighted by *b*) was set to the value one, and the rest of the *r* values were set to zero. Finally these binary-thresholded *r* values were plotted onto a surface model of the brain.

Eye and muscle activity analysis

To assess the contribution of eye activity to decoding, the decoding procedure was executed off-line with channels of vertical and horizontal EOG activity included with the 34 channels of EEG activity. The percent contribution of these eye channels was then assessed by dividing the absolute value of their regression weights by the sum of the absolute value of all the regression weights. To assess whether muscle activity inadvertently aided cursor control, we cross correlated EMG signals from flexor and extensor muscles of the right forearm with the *x* and *y* components of cursor velocity over 200 positive and negative lags (-2s to 2s in increments of 10ms). Prior to the cross correlation, the EMG signals were decimated 20 times after applying a 40 Hz low-pass antialiasing filter, rectified by taking the absolute value, low-pass filtered with a fourth-order, low-pass Butterworth filter at 1 Hz, and first-order differenced.

Results

Calibration

During the calibration phase, subjects tracked the movement of a computer-controlled cursor, and we subsequently calibrated the decoder based on the cursor velocity and EEG signals. We quantified the accuracy of each subject's calibrated decoder by computing the

mean of Pearson's *r* between measured and reconstructed cursor velocities across cross-validation folds (Fig. 3.3). Across subjects, the decoding accuracies for *x* and *y* velocities were correlated (r = 0.67) even though the decoding accuracy for *x* velocity was consistently higher than that for *y* velocity. The across-subject mean *r* values for *x* and *y* velocities were 0.68 and 0.50 respectively, indicating high decoding accuracy for observed cursor movement.

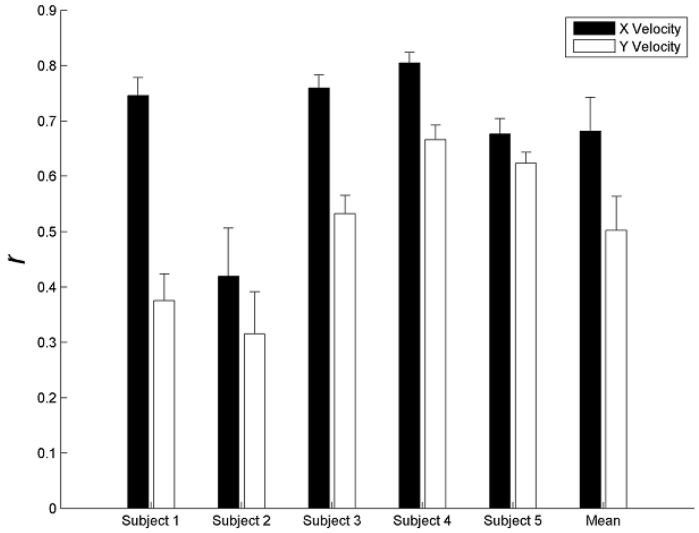

Fig. 3.3. EEG decoding accuracy of observed cursor velocity during the calibration phase. We computed the mean ± standard error (SE) of the decoding accuracies (*r* values) across cross-validation folds (n = 10) for each subject for *x* (black) and *y* (white) cursor velocities.

Scalp maps of sensor contributions to the reconstruction of observed cursor movements in the calibration phase depicted the contributions as a network of frontal, central, and parietal regions (Fig. 3.4). Within this network, sensors over the frontocentral (F1, FCZ) and primary sensorimotor cortices (CP1-CP4) made the greatest contribution. Concerning

time lags, EEG data from 50 ms in the past supplied the most information with 12.4% of the total contribution. In source space at 50 ms in the past, the precentral gyrus (PrG), postcentral gyrus (PoG), lateral premotor (LPM) cortex, superior temporal sulcus (STS), and dorsal and ventral portions of lateral prefrontal cortex (LPC) played a large role in the encoding of observed cursor velocity (Fig. 3.5).

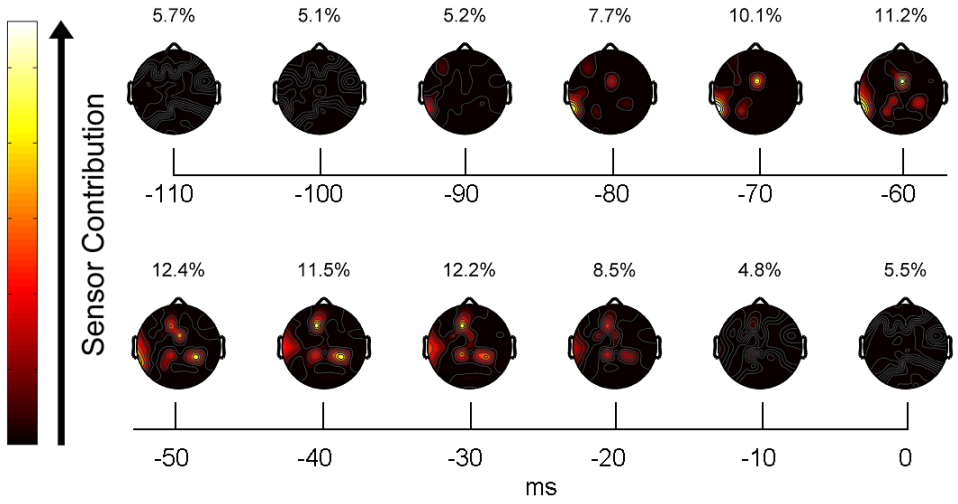

Fig. 3.4. Scalp sensor contributions to the reconstruction of observed cursor velocity during the calibration phase. Mean (n = 5) scalp maps of the sensors revealed a network of frontal, central, and parietal involvement. In particular, F1, FCZ, and CP1-CP4 made the largest contribution. Light and dark colors represent high and low contributors, respectively. Each scalp map with its percentage contribution is displayed above its associated 10 ms time lag, revealing the 12.4% maximal contribution of EEG data at 50 ms in the past.

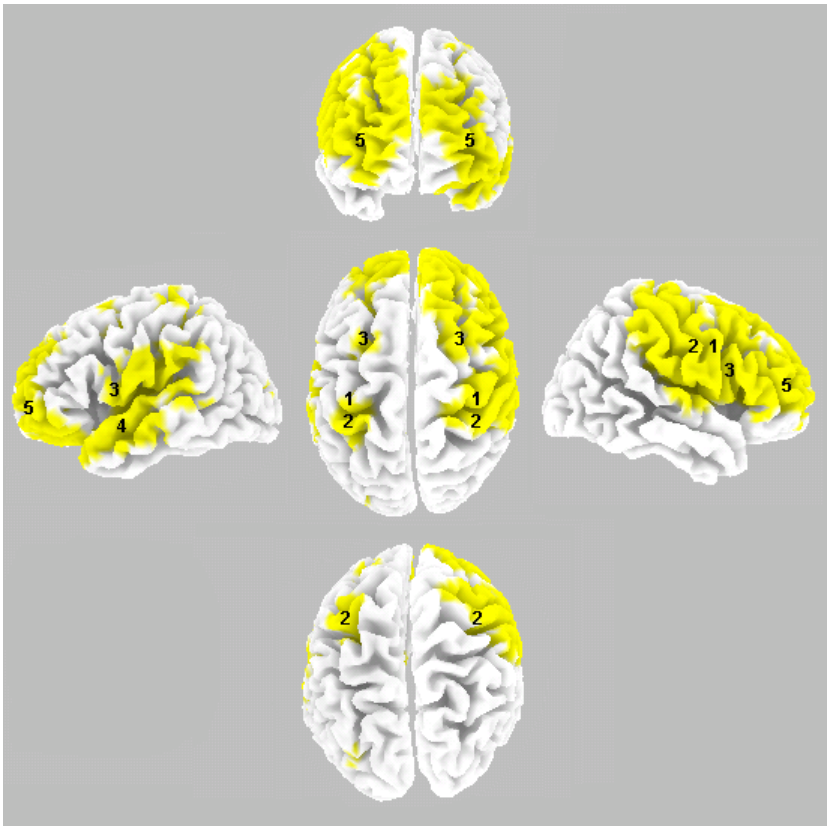

Fig. 3.5. Sources that maximally encoded observed cursor velocity during the calibration phase. We overlaid localized sources (yellow) from 50 ms in the past onto a model of the brain in different orientations to reveal the involvement of the PrG (1), PoG (2), LPM (3), STS (4), and dorsal and ventral LPC (5).

Target acquisition

During the target acquisition phase, subjects controlled the cursor with their EEG signals to hit targets that appeared one at a time pseudorandomly at the left, top, right, or bottom of the workspace. The length-normalized cursor paths confirmed the subjects' ability to move from the center to the target (Fig 3.6).

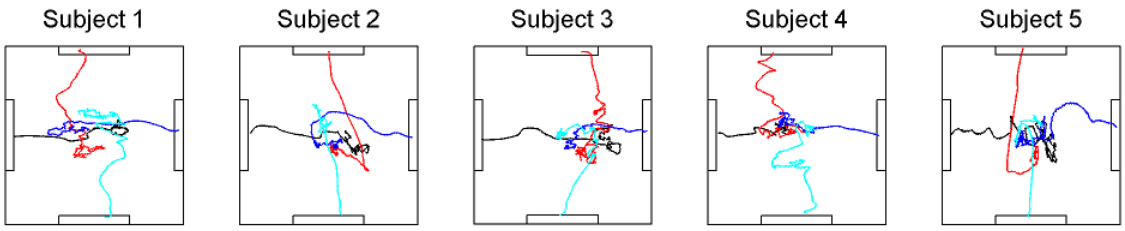

Fig. 3.6. Mean brain-controlled cursor paths. Each colored path is the mean of the length-normalized trials for a single direction (left, top, right, or bottom) across all trials of all runs for a subject. Trials in which subjects did not acquire the target within 15 s were not included in the analysis. The workspace dimensions were 30 x 30 cm.

For each target of each subject, the target hit rate and movement time (MT) across runs are given in Table 3.1. The overall means ± SE of the hit rate and MT were 73 ± 4% and 8.18 ± 0.18 s.

To examine whether subjects adapted across runs of the target acquisition phase, the target hit rate for all targets taken together was fitted across runs with a double exponential curve for each subject (Fig. 3.7). The hit rate of subjects 2 and 4 worsened initially and then began to improve. Only subjects 3 and 5 demonstrated clearly positive adaptation.

Table 3.1. Mean (SE) of the hit rate and MT for each target of each subject across runs (*n* = 4)

	Left		**Top**		**Right**		**Bottom**		**Mean**	
	Hit %	**MT**	**Hit %**	**MT**	**Hit %**	**MT**	**Hit %**	**MT**	**Hit %**	**MT**
Subject 1	94 (2)	7.30 (0.60)	66 (8)	8.80 (0.57)	98 (2)	7.43 (0.49)	55 (9)	10.7 (0.68)	78 (11)	8.56 (0.80)
Subject 2	83 (5)	8.97 (0.49)	96 (4)	7.70 (0.49)	85 (2)	7.68 (0.55)	85 (4)	7.12 (0.40)	87 (3)	7.87 (0.39)
Subject 3	84 (9)	7.51 (0.53)	45 (4)	11.8 (0.93)	100 (0)	5.50 (0.37)	67 (9)	8.89 (0.58)	74 (12)	8.44 (1.33)
Subject 4	71 (7)	6.86 (0.67)	33 (7)	9.49 (1.42)	65 (6)	9.87 (0.79)	21 (4)	8.59 (1.39)	47 (12)	8.70 (0.67)
Subject 5	57 (14)	10.0 (0.69)	100 (0)	5.58 (0.26)	60 (18)	9.06 (0.70)	100 (0)	4.59 (0.18)	79 (12)	7.32 (1.32)
Mean	78 (6)	8.13 (0.60)	68 (13)	8.69 (1.03)	81 (8)	7.91 (0.75)	65 (14)	7.98 (1.02)	73 (4)	8.18 (0.18)

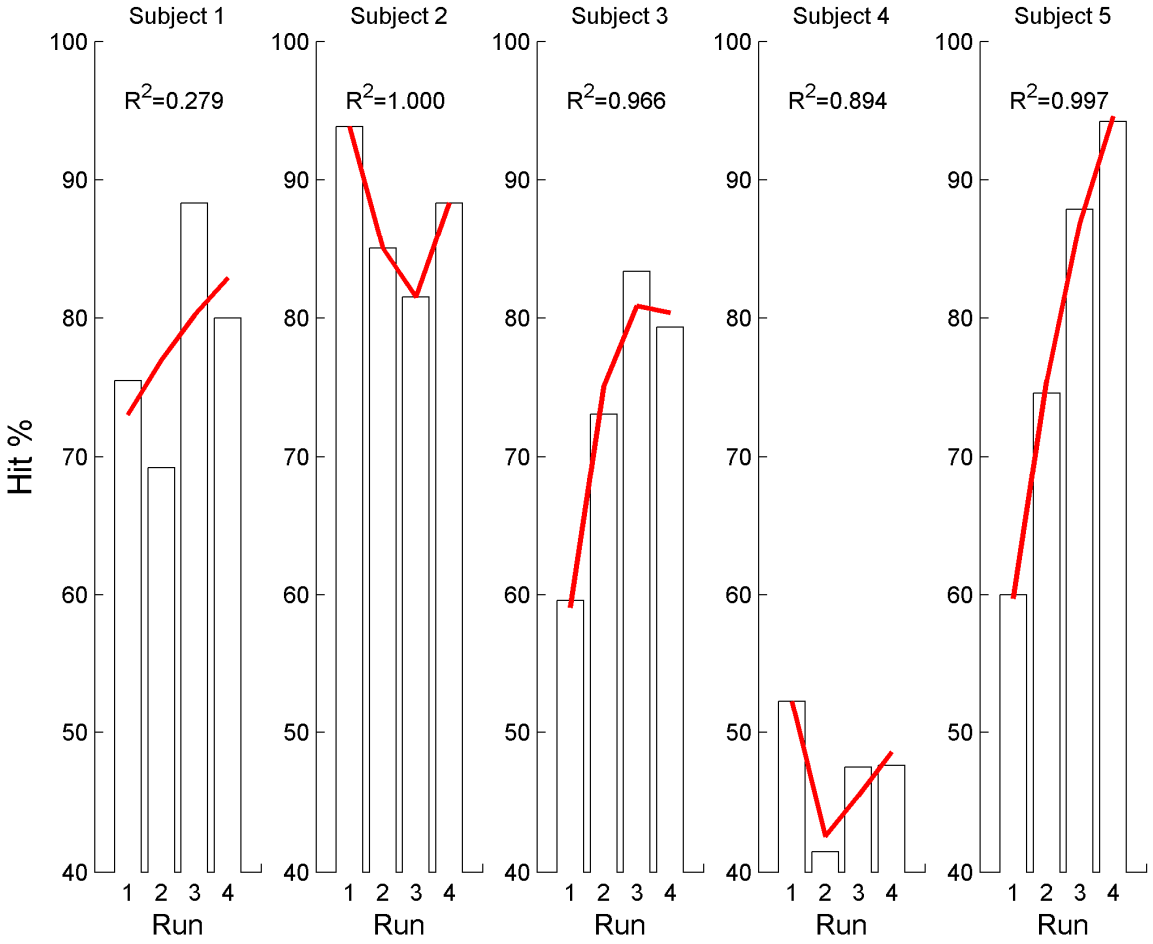

Fig. 3.7. Changes in target hit rate across runs. Each bar represents the target hit rate across targets. A double exponential curve was fitted to the target hit rates across runs for each subject (red). The coefficient of determination (R^2) of the fit is displayed within each subplot. Subjects 3 and 5 most clearly demonstrated positive adaptation across runs.

Scalp maps of sensor contributions to the brain-controlled cursor velocity were generated from the mean of each subject's best run in the target acquisition phase. They depicted the contributions as having shifted to be more focused within central regions (Fig. 3.8). As in the calibration phase, EEG data from 50 ms in the past supplied the most information with 12.1% of the total contribution. In source space at 50 ms in the past,

compared to the calibration phase, a large shift occurred from anterior (fronto-central) to posterior (centro-posterior) neural regions. More specifically, there was much less involvement of the LPC, the PrG and PoG exhibited an even more widespread involvement, and the inferior parietal lobule (IPL) made a large contribution (Fig. 3.9).

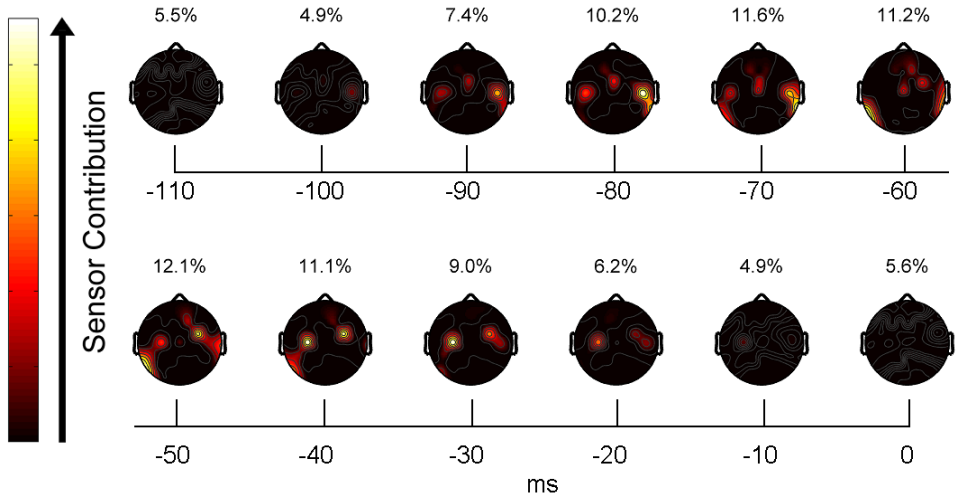

Fig. 3.8. Scalp sensor contributions to the brain-controlled cursor velocity during the target acquisition phase. Mean (n = 5) scalp maps of the sensors weights from the subjects' best runs revealed a network that had shifted to involve more central regions than the network of the calibration phase. Light and dark colors represent high and low contributors, respectively. Each scalp map with its percentage contribution is displayed above its associated 10 ms time lag, revealing the 12.1% maximal contribution of EEG data at 50 ms in the past.

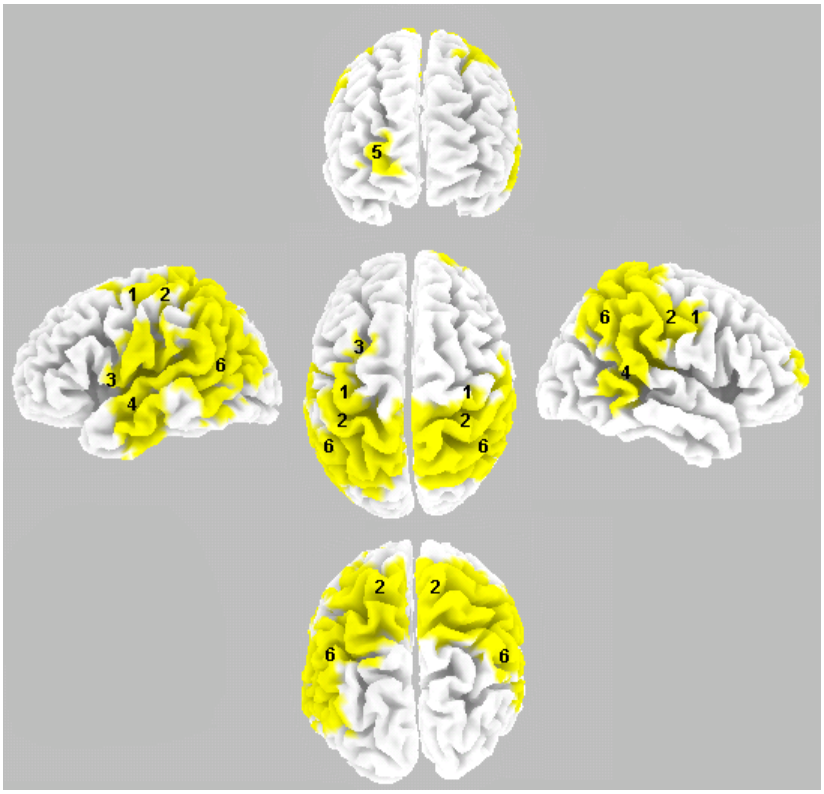

Fig. 3.9. Sources that maximally encoded brain-controlled cursor velocity during the target acquisition phase. We overlaid localized sources (yellow) from 50 ms in the past onto a model of the brain in different orientations to reveal a substantial involvement of PrG (1) and PoG (2) and some involvement of LPM (3). As in the calibration phase, the STS (4) was involved. In contrast to the calibration phase, the LPC (5) played a minor role, and the IPL (6) played a major role.

Contributions of eyes and muscles

A concern in BCI studies is that eye or muscle movements may contaminate EEG signals thereby inadvertently aiding the control of a device/environment that should be controlled by thought-generated neural signals alone. In the pilot testing for our study, we found that asking subjects to visually fixate the center of the workspace while simultaneously

tracking the cursor added attentional demands that burdened the subjects and likely compromised the decoding; therefore, we did not constrain eye movements. However, we executed the off-line decoding procedure with channels of vertical and horizontal EOG activity included, and assessed the percent contribution of these eye channels (Table 3.2.). The percent contributions were low for the calibration and target acquisition phases except for a very high percent contribution (94.9%) to *x* velocity reconstruction for Subject 4 during target acquisition. Interestingly, this subject had the lowest decoding accuracy of all participants, suggesting that eye movements disrupted decoding. To assess whether muscle activity aided cursor control, we cross correlated EMG signals from flexor and extensor muscles of the right forearm with the *x* and *y* components of cursor velocity to find that all correlations were low (Table 3.3.).

Table 3.2. Percent contribution of EOG activity to cursor velocity reconstruction

	Calibration		Target acquisition (best run)	
	X	**Y**	**X**	**Y**
Subject 1	0.30	1.58	0.00	0.01
Subject 2	0.00	0.01	0.20	0.18
Subject 3	1.99	9.60	1.54	0.47
Subject 4	0.00	0.01	94.9	0.04
Subject 5	0.34	0.65	0.06	0.03

Table 3.3. Mean (SD) of maximum absolute *r* values from cross correlation of forearm flexor and extensor EMG activity with *x* and *y* components of cursor velocity

	Calibration		Target acquisition (best run)	
	X	**Y**	**X**	**Y**
Flexor	0.05 (0.04)	0.05 (0.04)	0.04 (0.02)	0.07 (0.03)
Extensor	0.03 (0.02)	0.04 (0.01)	0.07 (0.08)	0.05 (0.04)

Discussion

In this study, we report the first EEG-based BCI system that employs continuous decoding of imagined continuous hand movements. Furthermore, we emphasize that the system requires only a single session of decoder calibration and subject practice (~40 min) before subjects can operate it. The off-line decoding results of the calibration phase that used observation of biologically plausible cursor movement were higher than those of invasive BCI studies and may imply, as discussed below, the involvement of a widespread MNS in humans. Also discussed below is the fact that, in the on-line target acquisition phase, subjects controlled a cursor with their EEG signals alone with accuracies comparable to other noninvasive and invasive BCI studies aimed at 2D cursor control.

Calibration

BCI systems are ultimately intended for movement impaired persons; therefore, it is important that the decoder calibration and/or subject training procedures not require overt movement. For this reason, we used a decoder calibration procedure similar to that described by Hochberg et al. (2006) that requires only observation of biologically plausible cursor movement. This type of training for BCI systems presumably engages the MNS, which predicts and interprets one's own actions and the actions of others (Tkach et al. 2008). In fact, neuronal activity acquired from intracortical microelectrode arrays implanted in the dorsal premotor cortex (PMd) and the arm area of the PrG (primary motor cortex, M1), common sites for BCI-related studies, exhibits qualities of mirror neurons during observation of cursor movements (Cisek and Kalaska 2004; Wahnoun et al. 2006; Tkach et al. 2007).

Current electrophysiological correlates of the putative human MNS, as acquired through EEG, are based on modulation of the mu rhythm (8–13 Hz), which exhibits suppression during action observation and action performance (Perry and Bentin 2009). These EEG correlates at the scalp level have been reported to be similar to those revealed by neural hemodynamics acquired with functional magnetic imaging (fMRI) (Perry and Bentin 2009). However, for examining, in spatial detail, the widespread networks of cortical regions that may compose the human MNS, arguably fMRI is considered by many to be the best tool. Since our examination of cortical sources that encoded observed cursor velocity revealed some regions commonly held to comprise the canonical human MNS (ventral LPM, STS, and LPC (Iacoboni and Dapretto 2006)) and regions reportedly

containing mirror neurons related to the task (PMd, M1) (Cisek and Kalaska 2004; Wahnoun et al. 2006; Tkach et al. 2007), our method may provide detailed temporal *and* spatial temporal information about the internal representations of both observed and executed actions, which is not provided by the study of mu rhythm dynamics or hemodynamics alone. Therefore, our approach may be suitable for future investigation into the development and plasticity of the hypothesized MNS in humans. Interestingly, that our subjects' mean decoding accuracy was double that of studies that acquired neural signals with intracranial microelectrode arrays (Kim et al. 2008; Truccolo et al. 2008) could be attributed to capturing more information for reconstruction by recording neural signals from an MNS network instead of only mirror neurons in M1. Our method also provides further evidence that the MNS is involved during observed cursor movement by indicating the presence of planning activity that peaks at 50 ms in the past, excluding the decoding of passive viewing as an explanation and suggesting predictive decoding informed by forward models (Miall 2003).

Target acquisition

Our study is the first noninvasive EEG-based BCI study to employ continuous decoding of imagined natural movement. Previous work in EEG-based BCI systems for cursor control required subjects to learn to modulate sensorimotor rhythms to move the cursor akin to neuro/biofeedback training. These studies based on sensorimotor rhythms required weeks to months of training before levels of performance were deemed sufficient for reporting (Wolpaw and McFarland 2004). We believe the fact that we used a decoder based on imagined/observed natural movement reduced the training

requirements of our study to only a single brief practice session (~20 min), a significant advancement. Table 3.4 compares our study to Wolpaw and McFarland (2004).

An ECoG study based on sensorimotor rhythms for 2D cursor control that had objectives similar to ours also observed that several subjects clearly adapted over a short period of time (Schalk et al. 2008). Although this ECoG study reduced training time compared to Wolpaw and McFarland (2004), some drawbacks included that pre-training time was still taken for the initial selection of control features and for training subjects to first move the cursor in one dimension at a time. We were able to bypass these two pre-training steps. Another drawback of the ECoG study was that all five subjects used overt movement for initial selection of features, and two subjects used overt movement throughout the study. Table 3.4 compares our study to Schalk et al. (2008).

The results of our target acquisition phase compare favorably to those in tetraplegic humans that were implanted with intracortical arrays in the arm area of M1 (Hochberg et al. 2006; Kim et al. 2008) even though the performance results of those studies (Table 3.4) were only computed on data collected weeks to months after training began.

Table 3.4. Comparison to most relevant human BCI studies of 2D cursor control

	Number of subjects	Neural data	Target size as % of workspace	Timeout (s)	Movement time (s)	Target hit %
Wolpaw and McFarland 2004	4	EEG	4.9	10	1.9	92
Hochberg et al. 2006	1	single units	NA	7	2.5	85
Kim et al. 2008	2	single units	1.7	7	3.1	75
Schalk et al. 2008	5	ECoG	7	16.8	2.4	63
Present study	5	EEG	1.3	15	8.2	73

Besides differences in training time, our study differs from the aforementioned studies in its reporting of cortical sources involved in encoding cursor control. The most notable differences between the regions that encoded for observed cursor velocity and brain-controlled cursor velocity were with the PrG, PoG, IPL, and LPC. There was a more widespread contribution from the PrG, PoG, and IPL during brain control, which could simply reflect the increased involvement of imagined motor execution (Miller et al. 2010) especially since these regions have previously been shown to be engaged in encoding cursor kinematics (Jerbi et al. 2007; Bradberry et al. 2009a). The contribution from the LPC was largely attenuated during brain-controlled cursor movements, suggesting a

transition out of the imitative learning environment of cursor observation (Vogt et al. 2007).

In the near future, it will be important for patients with impaired upper limb movement to test our noninvasive BCI system since they are the target population for this assistive technology. Since our results indicate that calibration of our decoder and initial subject practice require a short amount of time in a single session, we expect to avoid burdening patients with a lengthy training. Employing our method will also permit future investigations into the putative human MNS, potentially providing further insights into training protocols for BCI systems.

Funding

Financial support provided by the Office of Naval Research (N000140910126), La Fondation Motrice (Paris, France), and the Graduate Research Initiative Fund of the Department of Kinesiology at the University of Maryland.

Appendix A: Demographics and Institutional Review Board (IRB) approval

A.1. Demographics

The subjects of all studies were right-handed males between the ages of 18 and 45 recruited from the students and faculty of the University of Maryland at College Park.

A.2. IRB approval of human subjects research

A.2.1. MEG study of Chapter 1

IRB approval letter

UNIVERSITY OF MARYLAND
INSTITUTIONAL REVIEW BOARD

2100 Lee Building
College Park, Maryland 20742-5121
301.405.4212 TEL 301.314.1475 FAX

Reference: IRB HSR Identification Number 04-0152

March 24, 2004

MEMORANDUM

Notice of Results of Final Review by IRB on HSR Application

TO: Dr. Jose Contreras-Vidal
Bruce Swett
Feng Rong
Department of Kinesiology

FROM: Dr. Phylis Moser-Veillon, Co-Chairperson
Dr. Marc Rogers, Co-Chairperson
Institutional Review Board

PROJECT ENTITLED:
"EEG/MEG Study of Error Detection and Visuomotor Learning (Continuation of IRB/HSR PROTOCOL NUMBER 03-0120)"

The Institutional Review Board (IRB) concurs with the departmental Human Subjects Review Committee's (HSRC's) preliminary review of the application concerning the above referenced project. The IRB has approved the application and the research involving human subjects described therein. We ask that any future communications with our office regarding this research reference the IRB HSR identification number indicated above.

We also ask that you not make any changes to the approved protocol without first notifying and obtaining the approval of the IRB. Also, please report any deviations from the approved protocol to the Chairperson of your departmental HSRC. If you have any questions or concerns, please do not hesitate to contact us at irb@deans.umd.edu. Thank you.

ADDITIONAL INFORMATION REGARDING IRB/HSRC APPROVALS

EXPIRATION OF IRB APPROVAL—Approval of non-exempt projects expires one year after the official date of IRB approval; approval of exempt projects expires three years after that date. If you expect to be collecting or analyzing data after the expiration of IRB approval, please contact the HSRC Chairperson in your department about submitting a renewal application. **(PLEASE NOTE: If you are not collecting data from human subjects and any on-going data analysis does not increase the risk to subjects, a renewal application would not be necessary.)**

STUDENT RESEARCHERS—Unless otherwise requested, the IRB will send copies of approval paperwork to the supervising faculty researcher (or advisor) of a project. We ask that such persons pass on that paperwork or a copy to any student researchers working on that project. That paperwork may be needed by students in order to apply for graduation. **PLEASE BE ADVISED THAT THE IRB MAY NOT BE ABLE TO PROVIDE COPIES OF THAT PAPERWORK, particularly if several years have passed since the date of the original approval.**

Enclosures (where appropriate), will include stamped copy of informed consent forms included in application and any copies of the application not needed by the IRB; copies of this memorandum and any consent forms to be sent to the Chairperson of the Human Subjects Review Committee

IRB-stamped consent form

CONSENT FORM: Student

Cognitive Motor Behavior Laboratory
Department of Kinesiology
University of Maryland College Park

Initials _____ Date _____

Project Title: **EEG / MEG Study of Error Detection and Processing.**

Statement of Age of Participant: I hereby state that I am over 18 years of age, in good physical and emotional health, and would like to participate in a program of research being conducted by Professor Jose Contreras-Vidal, Ph.D., of the Department of Kinesiology at the University of Maryland , College Park, Maryland 20742, and associates.

Purpose of the Research Project: The purpose of the current research is to study how the brain detects errors, and modifies internal processes to correct them, in the young vs. the elderly; and in persons with Parkinson's disease vs. those with no known health conditions.

Procedures Used: **(Check which procedures will be used)**
General Procedures: All participants will complete a form to assess their physical health. Persons with a prior, medical diagnosis of Parkinson's disease will complete an additional form about their medication. A brief assessment of thinking abilities will be given, by asking a series of questions.

Task-Specific Procedures:
_____ EEG (Electroencephalograph). Participants will have a nylon cap with EEG sensors in it placed on their head. A gel that helps make the connection will be put on the Participant's head, where the contacts touch the scalp. Participants will sit in a comfortable chair, with his/her hand resting on a table. Participants will perform movement tasks, using a pen to draw on a tablet that records the movement. Participants will be asked to move the pen towards a target, while wearing a cap with EEG sensors on their head. The EEG sensors detect electrical activity at the scalp. The EEG does not put any electricity into a person's body. KNES498p students will be compensated with 1 lab participation credit (see section on Compensation below).

_____ MEG (Magnetoelectroencephalograph). Participants will lie on a bed inside a magnetically-shielded room for up to three hours. Participants will be asked to remove any metal objects (watches, belts, etc.), and their shoes. Participants will lie on the bed in a darkened room, looking at a computer image, while moving a pen across a glass surface. Participants will be asked to move the pen towards a target, while lying quietly with their head in the MEG recording device. Participants may rest their arms between trials. The MEG measures the magnetic fields created by activity in the brain. The MEG does not put any electricity into a person's body. KNES498p students will be compensated with 1 lab participation credit (see section on Compensation below).

Principal Investigator: Jose Contreras-Vidal, PhD Dept. of Kinesiology, 2363 HHP Bldg.
University of Maryland at College Park, College Park, MD 20742 Phone: 301-405-2495

CONSENT FORM: Student

Cognitive Motor Behavior Laboratory
Department of Kinesiology
University of Maryland College Park

Compensation: Students recruited from KNES498p will be offered the option to use participation in the study as an alternative to a lab / participation assignment (or may use participation in the study to replace their lowest lab / participation grade). Lab / participation accounts for 25% of the student's grade in KNES498p. Student participation is purely optional; there is no penalty for not participating in the study.

Confidentiality: All information collected in the study is confidential, and my name will not be identified at any time, or linked with the data collected (including data stored electronically). The data I provide will generally be grouped with data provided by others for reporting and presentation. Data collected will be secured in a locked filing cabinet in the Cognitive Motor Behavior Lab, in HHP.

Risks: I understand that as a result of sitting or lying still for a prolonged period of time, I may experience some discomfort. Also, in the MEG study, I will be lying on my back in an enclosed, dimly lit room for the duration of the study. There are no other known risks. The MEG device does not generate magnetic fields, it records the magnetic fields that are naturally generated by my own brain's activity.

Benefits: I understand that the research study is not designed to help me personally, either physically or emotionally. The study is intended to further our understanding of voluntary movement, error detection, brain functioning, and Parkinson's disease.

Freedom to Withdraw: I understand that I am free to ask questions about the study, or to withdraw from the study at any time, without penalty.

I understand that the University of Maryland does not provide any medical care or hospitalization insurance coverage for participants in this research study; nor will the University of Maryland pay any medical expenses or provide any compensation for any injury sustained as a result of participation in this research study, except as required by law.

Informed Consent: *"I am voluntarily making a decision whether or not participate in the research study described above. My signature indicates that I have decided to participate having read the information provided above and having had all of my questions answered. I will be given a copy of this consent form to keep."*

Printed Name of Participant: _____ Signature of Participant: _____

Signature of Witness: _____ Date of Signatures: _____

Principal Investigator: Jose Contreras-Vidal, PhD Dept. of Kinesiology, 2363 HHP Bldg.
University of Maryland at College Park, College Park, MD 20742 Phone: 301-405-2495

A.2.2. EEG studies of Chapters 2 and 3

IRB approval letter

January 25, 2010

To:	**Investigator:** Jose Luis Contreras-Vidal **Co-Investigator(s):** Not Applicable **Student Investigator:** Trent Jason Bradberry **Department:** KNES - Kinesiology
From:	Joseph M. Smith, MA, CIM Manager University of Maryland, College Park
Re:	**IRB Application Number:** 06-0031 (PAS# 1954.4) **Project Title:** "Non-invasive neural prosthetics for reaching"
Approval Date:	01-22-2010
Expiration Date:	01-22-2011
Type of Application:	Renewal
Type of Research:	Non-Exempt
Type of Review:	Expedited

The University of Maryland, College Park Institutional Review Board (IRB) approved your IRB application. The research was approved in accordance with the University's IRB policies and procedures and 45 CFR 46, the Federal Policy for the Protection of Human Subjects. Please reference the above-cited IRB application number in any future communications with our office regarding this research.

Recruitment/Consent: For research requiring written informed consent, the IRB-approved and stamped informed consent document is enclosed. The IRB approval expiration date has been stamped on the informed consent document. Please keep copies of the consent forms used for this research for three years after the completion of the research.

Continuing Review: If you want to continue to collect data from human subjects or analyze data from human subjects after the expiration date for this approval, you must submit a renewal application to the IRB Office at least 30 days before the approval expiration date.

Modifications: Any changes to the approved protocol must be approved by the IRB before the change is implemented except when a change is necessary to eliminate apparent immediate hazards to the subjects. If you want to modify the approved protocol, please submit an IRB addendum application to the IRB Office.

Unanticipated Problems Involving Risks: You must promptly report any unanticipated problems involving risks to subjects or others to the IRB Manager at 301-405-0678 or jsmith@umresearch.umd.edu.

Student Researchers: Unless otherwise requested, this IRB approval document was sent to the Principal Investigator (PI). The PI should pass on the approval document or a copy to the student researchers. This IRB approval document may be a requirement for student researchers applying for graduation. The IRB may not be able to provide copies of the approval documents if several years have passed since the date of the original approval.

Additional Information: Please contact the IRB Office at 301-405-4212 if you have any IRB-related questions or concerns.

IRB-stamped consent form

Initials _____ Date _____

CONSENT FORM

Project Title	Non-invasive neural prosthetics for reaching
Why is this research being done?	This is a research project being conducted by José L. Contreras-Vidal, Ph.D., Trent Bradberry, Harshavardhan Agashe, and Rodolphe Gentili, Ph.D., at the University of Maryland, College Park. We are inviting you to participate in this research project because you are an 18 – 65 year old, healthy, right-handed person residing in the greater Washington, DC area. The purpose of this research project is to develop non-invasive neural prosthetics that will improve the quality of life of individuals with impaired movement of their upper limbs due to injury or disease.
What will I be asked to do?	You will be asked to perform the *checked* procedure in the Cognitive Motor Neuroscience Lab in the Health and Human Performance Building: ☐ Procedure 1: Data Collection You will be asked to do the following during the preparation stage (1 hour): 1. Fill out a form with your personal health information. 2. Have your head fitted with an electroencephalography (EEG) cap with up to 128 hollow sensors. The sensors will be filled with conductive gel to ensure good physical contact with your scalp. 3. Have a reference sensor placed on your ear. 4. Have eye activity recorded with sensors around your right eye. 5. Have your head stabilized with a chin rest to minimize head movement. 6. Have 6 infrared emitting diode (IRED) markers placed on your reaching arm. The marker will be visible only to the camera system used to track the movement of your finger. 7. Wear a data-collection glove. You will be asked to perform either (a) or (b) indicated below: (a) Reaching movements to 8 targets using the following instructions (45 minutes): 1. Press the center target. 2. In your mind, select one of the 8 targets. 3. Reach to your selected target. 4. After you have reached the target, return your hand to the center position. 5. After 20 practice trials, there will be 40 trials per target for a total of 320 trials. 6. You may rest between any trials without negatively affecting the study. (b) Reaching movements to and grasping 8 objects or tools using the following instructions (45 minutes) 1. Start with your arm in the resting position. 2. In your mind, select one of the 8 objects or tools. 3. When the indicator light turns green, reach and grasp the selected object. 4. Return your hand to the resting position. 5. After 20 practice trials, there will be 40 trials per target for a total of 320 trials. 6. You may rest between any trials without negatively affecting the study. You will be paid $20 and may be invited back to perform Procedure 2

Initials _____ Date _____

Project Title	Non-invasive neural prosthetics for reaching
What will I be asked to do? (continued)	☐ Procedure 2: Testing of Computer Cursor Control by Experienced Subjects You will be asked to do the following during the preparation stage (1 hour): 1. Fill out a form with your personal health information. 2. Have your head fitted with an electroencephalography (EEG) cap with up to 64 hollow sensors. The sensors will be filled with conductive gel to ensure good physical contact with your scalp. 3. Have a reference sensor placed on your ear. 4. Have eye activity recorded with sensors around your right eye. 5. Have your head stabilized with a chin rest to minimize head movement. 6. Have electromyography (EMG) sensors placed on the skin of your arm and shoulder with double-sided adhesive tape. Specifically the sensors will be positioned over two muscles responsible for moving your upper arm (anterior and posterior deltoids) and two muscles responsible for moving your forearm (biceps and triceps). The sensors are used for recording the inadvertent muscle activity you may generate. You will be asked to perform *imagined* reaching movements to 8 targets using the following instructions (45 minutes): 1. Keep your hand and arm stationary throughout the entire experiment. 2. Watch the computer cursor move to the target on the computer screen as you continue to *imagine* reaching to the actual target. 3. If you accidentally acquire the wrong target, verbally say so. 4. Think about your hand being in a center position. 5. Watch the computer cursor move to the center position on the computer screen as you continue to *imagine* reaching to the center position. 6. The task will end when you reach 160 times or 45 minutes elapse, which ever occurs first. 7. You may rest between any trials without negatively affecting the study. You will be paid $10 plus $0.16 for each trial completed in less than 10 seconds for a maximum payment of $20. You may be invited back to perform Procedure 3. ☐ Procedure 3: Testing of Robotic Arm Control by Experienced Subjects You will be asked to do the following during the preparation stage (1 hour): 1. Fill out a form with your personal health information. 2. Have your head fitted with an electroencephalography (EEG) cap with up to 64 hollow sensors. The sensors will be filled with conductive gel to ensure good physical contact with your scalp. 3. Have a reference sensor placed on your ear. 4. Have eye activity recorded with sensors around your right eye. 5. Have your head stabilized with a chin rest to minimize head movement. 6. Have electromyography (EMG) sensors placed on the skin of your arm and shoulder with double-sided adhesive tape. Specifically the sensors will be positioned over two muscles responsible for moving your upper arm (anterior and posterior deltoids) and two muscles responsible for moving your forearm (biceps and triceps). The sensors are used for recording the inadvertent muscle activity you may generate.

Initials _____ Date _____

Project Title	Non-invasive neural prosthetics for reaching
What will I be asked to do? (continued)	You will be asked to perform *imagined* reaching movements to 8 targets using the following instructions (45 minutes): 1. Keep your hand and arm stationary throughout the entire experiment. 2. Watch the robotic arm move to the target as you continue to *imagine* reaching to it. 3. If you accidentally acquire the wrong target, verbally say so. 4. Think about your hand being in a center position. 5. Watch the robotic arm move to the center position as you continue to *imagine* reaching to the center position. 6. The task will end when you reach 160 times or 45 minutes elapse, which ever occurs first. 7. You may rest between any trials without negatively affecting the study. You will be paid $10 plus $0.16 for each trial completed in less than 10 seconds for a maximum payment of $20. ☐ Procedure 4: Testing of Robotic Arm Control by Novice Subjects You will be asked to do the following during the preparation stage (1 hour): 1. Fill out a form with your personal health information. 2. Have your head fitted with an electroencephalography (EEG) cap with 32 to 64 hollow sensors. The sensors will be filled with conductive gel to ensure good physical contact with your scalp. 3. Have a reference sensor placed on your ear. 4. Have eye activity recorded with sensors around your right eye. 5. Have your head stabilized with a chin rest to minimize head movement. 6. Have electromyography (EMG) sensors placed on the skin of your arm and shoulder with double-sided adhesive tape. Specifically the sensors will be positioned over two muscles responsible for moving your upper arm (anterior and posterior deltoids) and two muscles responsible for moving your forearm (biceps and triceps). The sensors are used for recording the inadvertent muscle activity you may generate. You will be asked to perform *imagined* reaching movements to 8 targets using the following instructions (45 minutes): 1. Keep your hand and arm stationary throughout the entire experiment. 2. Watch the robotic arm move to the target as you continue to *imagine* reaching to it. 3. If you accidentally acquire the wrong target, verbally say so. 4. Think about your hand being in a center position. 5. Watch the robotic arm move to the center position as you continue to *imagine* reaching to the center position. 6. The task will end when you reach 160 times or 45 minutes elapse, which ever occurs first. 7. You may rest between any trials without negatively affecting the study. You will be paid $10 plus $0.16 for each trial completed in less than 10 seconds for a maximum payment of $20.

Initials _____ Date _____

Project Title	Non-invasive neural prosthetics for reaching
What about confidentiality?	We will do our best to keep your personal information confidential. To help protect your confidentiality, names will not be identified at any time or linked with the data collected (including data stored electronically). A code will be placed on the survey and other collected data. The data provided will generally be grouped with data provided by others for reporting and presentation. Data collected will be secured in a locked filing cabinet in the Cognitive Motor Neuroscience Lab, in the Health and Human Performance Building. Only the Principal Investigator and his collaborators will have access to this locked file cabinet. If we write a report or article about this research project, your identity will be protected to the maximum extent possible. This research project involves making videotapes of you. The videotapes will only be used by the investigators to confirm your movements if there are issues with the data obtained from the other recording equipment. The videotapes will be secured with the other data as described above. These videotapes will be destroyed when the study concludes. ___ I agree to be videotaped during my participation in this study ___ I do not agree to be videotaped during my participation in this study
What are the risks of this research?	You may experience a mild degree of physical discomfort due to prolonged sitting during the EEG cap preparation time and experiment time and removal of the adhesive securing the hand markers and EMG sensors, mental fatigue due to concentration, and/or physical fatigue in the reaching arm if participating in Procedure 1.
What are the benefits of this research?	You will not personally benefit from this study; however, individuals with impaired upper limb movement will greatly benefit from the proposed research. The ability to manipulate the environment will be restored to the motor-disabled population by the use of the thought-controlled neural prosthetic devices developed from this study.
Do I have to be in this research? May I stop participating at any time?	Your participation in this research is completely voluntary. You may choose not to take part at all. If you decide to participate in this research, you may stop participating at any time. If you decide not to participate in this study or if you stop participating at any time, you will not be penalized or lose any benefits to which you otherwise qualify.
Is any medical treatment available if I am injured?	The University of Maryland does not provide any medical, hospitalization, or other insurance for participants in this research study, nor will the University of Maryland provide any medical treatment or compensation for any injury sustained as a result of participation in this research study, except as required by law.
What if I have questions?	This research is being conducted by José L. Contreras-Vidal, Ph.D., Trent Bradberry and Harshavardhan Agashe at the University of Maryland, College Park. If you have any questions about the research study itself, please contact José L. Contreras-Vidal at 301-405-2495 or pepeum@umd.edu. If you have questions about your rights as a research subject or wish to report a research-related injury, please contact: **Institutional Review Board Office, University of Maryland, College Park, Maryland, 20742; irb@deans.umd.edu; 301-405-0678** This research has been reviewed according to the University of Maryland, College Park IRB procedures for research involving human subjects.
Statement of Age of Subject and Consent	Your signature indicates that: you are at least 18 years of age the research has been explained to you your questions have been fully answered you freely and voluntarily choose to participate in this research project
Signature and Date	NAME OF SUBJECT SIGNATURE OF SUBJECT DATE

IRB APPROVED
EXPIRES ON
JAN 22 2011
UNIVERSITY OF MARYLAND
COLLEGE PARK

References

Alpaydin E (2004) Introduction to machine learning, p 254. Cambridge, MA: MIT.

Averbeck BB, Chafee MV, Crowe DA, Georgopoulos AP (2005) Parietal representation of hand velocity in a copy task. J Neurophysiol 93:508–518.

Averbeck BB, Crowe DA, Chafee MV, Georgopoulos AP (2009) Differential contribution of superior parietal and dorsal–lateral prefrontal cortices in copying. Cortex 45:432–441.

Birbaumer N, Elbert T, Canavan AG, Rockstroh B (1990) Slow potentials of the cerebral cortex and behavior. Physiol Rev 70:1– 41.

Bradberry TJ, Contreras-Vidal JL, Rong F (2008) Decoding hand and cursor kinematics from magnetoencephalographic signals during tool use. Conf Proc IEEE Eng Med Biol Soc 2008:5306 –5309.

Bradberry TJ, Rong F, Contreras-Vidal JL (2009a) Decoding center-out hand velocity from MEG signals during visuomotor adaptation. NeuroImage 47:1691–1700.

Bradberry TJ, Gentili RJ, Contreras-Vidal JL (2009b) Decoding three-dimensional hand kinematics from electroencephalographic signals. Conf Proc IEEE Eng Med Biol Soc 2009:5010 –5013.

Bradberry TJ, Gentili RJ, Contreras-Vidal JL (2010) Reconstructing three-dimensional hand movements from noninvasive electroencephalographic signals. J Neurosci 30:3432–7.

Burnod Y, Baraduc P, Battaglia-Mayer A, Guigon E, Koechlin E, Ferraina S, Lacquaniti F, Caminiti R (1999) Parieto-frontal coding of reaching: an integrated framework. Exp Brain Res 129:325–346.

Cisek P, Kalaska JF (2004) Neural correlates of mental rehearsal in dorsal premotor cortex. Nature 431:993–6.

Cohen D, Nicolelis MA (2004) Reduction of single-neuron firing uncertainty by cortical ensembles during motor skill learning. J Neurosci 24:3574 –3582.

Contreras-Vidal JL, Kerick SE (2004) Independent component analysis of dynamic brain responses during visuomotor adaptation. NeuroImage 21:936–945.

Efron B, Tibshirani RJ (1998) An introduction to the bootstrap. Boca Raton, FL: CRC.

Delorme A, Makeig S (2004) EEGLAB: an open source toolbox for analysis of singletrial EEG dynamics including independent component analysis. J Neurosci Methods 134:9–21.

Fuchs M, Kastner J, Wagner M, Hawes S, Ebersole JS (2002) A standardized boundary element method volume conductor model. Clin Neurophysiol 113:702–712.

Ganguly K, Carmena JM (2009) Emergence of a stable cortical map for neuroprosthetics control. PLoS Biol 7:e1000153.

Georgopoulos, A.P., Schwartz, A.B., Kettner, R.E., 1986. Neuronal population coding of movement direction. Science 233, 1416–1419.

Georgopoulos AP, Langheim FJ, Leuthold AC, Merkle AN (2005) Magnetoencephalographic signals predict movement trajectory in space. Exp Brain Res 167:132–135.

Ghilardi M, Ghez C, Dhawan V, Moeller J, Mentis M, Nakamura T, Antonini A, Eidelberg D (2000) Patterns of regional brain activation associated with different forms of motor learning. Brain Res 871:127–145.

Gourtzelidis P, Smyrnis N, Evdokimidis I, Balogh A (2001) Systematic errors of planar arm movements provide evidence for space categorization effects and interaction of multiple frames of reference. Exp Brain Res 139:59–69.

Graydon FX, Friston KJ, Thomas CG, Brooks VB, Menon RS (2005) Learning-related fMRI activation associated with a rotational visuo-motor transformation. Brain Res Cogn Brain Res 22:373–383.

Gu Y, Farina D, Murguialday AR, Dremstrup K, Montoya P, Birbaumer N (2009) Offline identification of imagined speed of wrist movements in paralyzed ALS patients from single-trial EEG. Front Neuroprosth 1:1–7.

Hammon PS, Makeig S, Poizner H, Todorov E, de Sa VR (2008) Predicting reaching targets from human EEG. IEEE Signal Proc Mag 25:69–77.

Hochberg LR, Serruya MD, Friehs GM, Mukand JA, Saleh M, Caplan AH, Branner A, Chen D, Penn RD, Donoghue JP (2006) Neuronal ensemble control of prosthetic devices by a human with tetraplegia. Nature 442:164–171.

Holmes CJ, Hoge R, Collins L, Woods R, Toga AW, Evans AC (1998) Enhancement of MR images using registration for signal averaging. J Comput Assist Tomogr 22:324–333.

Iacoboni M, Dapretto M (2006) The mirror neuron system and the consequences of its dysfunction. Nat Rev Neurosci 7:942–51.

Inoue K, Kawashima R, Satoh K, Kinomura S, Sugiura M, Goto R, Ito M, Fukuda H (2000). A PET study of visuomotor learning under optical rotation. NeuroImage 11:505–516.

Jerbi K, Lachaux JP, N'Diaye K, Pantazis D, Leahy RM, Garnero L, Baillet S (2007) Coherent neural representation of hand speed in humans revealed by MEG imaging. Proc Natl Acad Sci USA 104:7676–7681.

Kelso JA, Fuchs A, Lancaster R, Holroyd T, Cheyne D, Weinberg H (1998) Dynamic cortical activity in the human brain reveals motor equivalence. Nature 392:814–818.

Kettner RE, Schwartz AB, Georgopoulos AP (1988) Primate motor cortex and free arm movements to visual targets in three-dimensional space. III. Positional gradients and population coding of movement direction from various movement origins. J Neurosci 8:2938–2947.

Kim SP, Sanchez JC, Rao YN, Erdogmus D, Carmena JM, Lebedev MA, Nicolelis MA, Principe JC (2006) A comparison of optimal MIMO linear and nonlinear models for brain–machine interfaces. J Neural Eng 3:145–161.

Kim SP, Simeral JD, Hochberg LR, Donoghue JP, Black MJ (2008) Neural control of computer cursor velocity by decoding motor cortical spiking activity in humans with tetraplegia. J Neural Eng 5:455–76.

Krakauer JW, Ghilardi MF, Mentis M, Barnes A, Veytsman M, Eidelberg D, Ghez C (2004) Differential cortical and subcortical activations in learning rotations and gains for reaching: a PET study. J Neurophysiol 2:924–933.

Lebedev MA, Nicolelis MA (2006) Brain–machine interfaces: past, present and future. Trends Neurosci 29:536–546.

Lebedev MA, Carmena JM, O'Doherty JE, Zacksenhouse M, Henriquez CS, Principe JC, Nicolelis MA (2005) Cortical ensemble adaptation to represent velocity of an artificial actuator controlled by a brain–machine interface. J Neurosci 25:4681–4693.

Leuthardt EC, Schalk G, Wolpaw JR, Ojemann JG, Moran DW (2004) A brain–computer interface using electrocorticographic signals in humans. J Neural Eng 1:63–71.

McFarland DJ, Krusienski DJ, Sarnacki WA, Wolpaw JR (2008) Emulation of computer mouse control with a noninvasive brain–computer interface. J Neural Eng 5:101–110.

Mehring C, Rickert J, Vaadia E, Cardosa de Oliveira S, Aertsen A, Rotter S (2003) Inference of hand movements from local field potentials in monkey motor cortex. Nat Neurosci 6:1253–1254.

Mehring C, Nawrot MP, Cardosa de Oliveira S, Vaadia E, Schulze-Bonhage A, Aertsen A, Ball T (2004) Comparing information about arm movement direction in single

channels of local and epicortical field potentials from monkey and human motor cortex. J Physiol Paris 98:498–506.

Mellinger J, Schalk G, Braun C, Preissl H, Rosenstiel W, Birbaumer N, Kübler A (2007) An MEG-based brain–computer interface (BCI). NeuroImage 36:581–593.

Miall RC (2003) Connecting mirror neurons and forward models. NeuroReport 14:2135–7.

Miller KJ, Schalk G, Fetz EE, den Nijs M, Ojemann JG, Rao RP (2010) Cortical activity during motor execution, motor imagery, and imagery-based online feedback. Proc Natl Acad Sci U S A 107:4430–5.

Moran DW, Schwartz AB (1999) Motor cortical activity during drawing movements: population representation during spiral tracing. J Neurophysiol 82:2693–2704.

Mulliken GH, Musallam S, Andersen RA (2008) Decoding trajectories from posterior parietal cortex ensembles. J Neurosci 28:12913–12926.

O'Suilleabhain PE, Lagerlund TD, Matsumoto JY (1999) Cortical potentials at the frequency of absolute wrist velocity become phase-locked during slow sinusoidal tracking movements. Exp Brain Res 126:529–535.

Paninski L, Fellows MR, Hatsopoulos NG, Donoghue JP (2003) Spatiotemporal tuning of motor cortical neurons for hand position and velocity. J Neurophysiol 91:515–532.

Pascual-Marqui RD (2002) Standardized low-resolution brain electromagnetic tomography (sLORETA): technical details. Methods Find Exp Clin Pharmacol 24 (Suppl D):5–12.

Perry A, Bentin S (2009) Mirror activity in the human brain while observing hand movements: a comparison between EEG desynchronization in the mu-range and previous fMRI results. Brain Res 1282:126–32.

Pfurtscheller G, Brunner C, Schlögl A, Lopes da Silva FH (2006) Mu rhythm (de) synchronization and EEG single-trial classification of different motor imagery tasks. NeuroImage 31:153–159.

Pistohl T, Ball T, Schulze-Bonhage A, Aertsen A, Mehring C (2008) Prediction of arm movement trajectories from ECoG-recordings in humans. J Neurosci Methods 167:105–114.

Rickert J, Cardosa de Oliveira S, Vaadia E, Aertsen A, Rotter S, Mehring C (2005) Encoding of movement direction in different frequency ranges of motor cortical local field potentials. J Neurosci 25:8815–8824.

Rong F, Contreras-Vidal JL (2006) Magnetoencephalographic artifact identification and automatic removal based on independent component analysis and categorization approaches. J Neurosci Methods 157:337–354.

Sanchez JC, Carmena JM, Lebedev MA, Nicolelis MA, Harris JG, Principe JC (2004) Ascertaining the importance of neurons to develop better brain–machine interfaces. IEEE Trans Biomed Eng 51:943–953.

Sanchez JC, Gunduz A, Carney PR, Principe JC (2008) Extraction and localization of mesoscopic motor control signals for human ECoG neuroprosthetics. J Neurosci Methods 167:63–81.

Sandwell DT (1987) Biharmonic spline interpolation of GEOS-3 and SEASAT altimeter data. Geophys Res Lett 2:139–142.

Santhanam G, Ryu SI, Yu BM, Afshar A, Shenoy KV (2006) A high-performance brain–computer interface. Nature 442:195–198.

Schalk G, McFarland D J, Hinterberger T, Birbaumer N, Wolpaw JR (2004) BCI2000: a general-purpose brain-computer interface (BCI) system. IEEE Trans Biomed Eng 51:1034–43.

Schalk G, Kubánek J, Miller KJ, Anderson NR, Leuthardt EC, Ojemann JG, Limbrick D, Moran D, Gerhardt LA, Wolpaw JR (2007) Decoding two-dimensional movement trajectories using electrocorticographic signals in humans. J Neural Eng 4:264–275.

Schalk G, Miller KJ, Anderson NR, Wilson JA, Smyth MD, Ojemann JG, Moran DW, Wolpaw JR, Leuthardt EC (2008) Two-dimensional movement control using electrocorticographic signals in humans. J Neural Eng 5:75–84.

Scherberger H, Jarvis MR, Andersen RA (2005) Cortical local field potential encodes movement intentions in the posterior parietal cortex. Neuron 46:347–354.

Schwartz AB, Taylor DM, Helms Tillery SI (2001) Extraction algorithms for cortical control of arm prosthetics. Curr Opin Neurobiol 11:701–707.

Schwartz AB, Moran DW, Reina GA (2004) Differential representation of perception and action in the frontal cortex. Science 303:380–383.

Scott SH (2008) Inconvenient truths about neural processing in primary motor cortex. J Physiol 5:1217–1224.

Seidler RD, Noll DC, Chintalapati P (2006) Bilateral basal ganglia activation associated with sensorimotor adaptation. Exp Brain Res 175:544–555.

Serruya MD, Hatsopoulos NG, Paninski L, Fellows MR, Donoghue JP (2002) Instant neural control of a movement signal. Nature 416:141–142.

Talairach J, Tournoux P (1988) Co-planar Stereotaxic Atlas of the Human Brain: 3-Dimensional Proportional System — An Approach to Cerebral Imaging. New York, NY:Thieme Medical Publishers.

Tankus A, Yeshurun Y, Flash T, Fried I (2009) Encoding of speed and direction of movement in the human supplementary motor area. J Neurosurg 110:1304–1316.

Taylor DM, Helms Tillery SI, Schwartz AB (2002) Direct cortical control of 3D neuroprosthetic devices. Science 296:1829–1832.

Tkach D, Reimer J, Hatsopoulos NG (2007) Congruent activity during action and action observation in motor cortex. J Neurosci 27:13241–50.

Tkach D, Reimer J, Hatsopoulos NG (2008) Observation-based learning for brain-machine interfaces. Curr Opin Neurobiol 18:589–94.

Truccolo W, Friehs GM, Donoghue JP, Hochberg LR (2008) Primary motor cortex tuning to intended movement kinematics in humans with tetraplegia. J Neurosci 28:1163–1178.

Turner RS, Grafton ST, Votaw JR, Delong MR, Hoffman JM (1998) Motor subcircuits mediating the control of movement velocity: a PET study. J Neurophysiol 80:2162–2176.

van Hemmen JL, Schwartz AB (2008) Population vector code: a geometric universal as actuator. Biol Cybern 98:509–518.

Velliste M, Perel S, Spalding MC, Whitford AS, Schwartz AB (2008) Cortical control of a prosthetic arm for self-feeding. Nature 453:1098–1101.

Vogt S, Buccino G, Wohlschläger AM, Canessa N, Shah NJ, Zilles K, Eickhoff SB, Freund HJ, Rizzolatti G, Fink GR (2007) Prefrontal involvement in imitation learning of hand actions: effects of practice and expertise. NeuroImage 37:1371–83.

Wahnoun R, He J, Helms Tillery SI (2006) Selection and parameterization of cortical neurons for neuroprosthetic control. J Neural Eng 3:162–71.

Waldert S, Preissl H, Demandt E, Braun C, Birbaumer N, Aertsen A, Mehring C (2008) Hand movement direction decoded from MEG and EEG. J Neurosci 28:1000–1008.

Wessberg J, Stambaugh CR, Kralik JD, Beck PD, Laubach M, Chapin JK, Kim J, Biggs SJ, Srinivasan MA, Nicolelis MA (2000) Real-time prediction of hand trajectory by ensembles of cortical neurons in primates. Nature 408:361–365.

Wise SP, Boussaoud D, Johnson PB, Caminiti R (1997) Premotor and parietal cortex: corticocortical connectivity and combinatorial computations. Annu Rev Neurosci 20:25–42.

Wolpaw JR, McFarland DJ (2004) Control of a two-dimensional movement signal by a noninvasive brain–computer interface in humans. Proc Natl Acad Sci USA 101-17849–17854.

Wu W, Hatsopoulos N (2006) Evidence against a single coordinate system representation in the motor cortex. Exp Brain Res 175:197–210.

Wu W, Hatsopoulos NG (2007) Coordinate system representations of movement direction in the premotor cortex. Exp Brain Res 176:652– 657.